Geophysical Journal International

Geophys. J. Int. (2011) doi: 10.1111/j.1365-246X.2011.05235.x

Anisotropic Pn tomography of Turkey and adjacent regions

Ahu Kömeç Mutlu and Hayrullah Karabulut

Kandilli Observatory and Earthquake Research Institute, Boğaziçi University, Çengelköy, Istanbul, Turkey. E-mail: kara@boun.edu.tr

Accepted 2011 September 17. Received 2011 September 17; in original form 2011 February 11

SUMMARY

This study presents an analysis of Pn traveltimes to determine lateral variations of velocity, anisotropy of uppermost mantle and crustal thickness beneath Turkey and adjacent regions. From 1999 to 2010, more than 50 000 Pn arrivals are compiled from 700 regional earthquakes and 832 stations of permanent and temporary networks operated in the study area. We used a regularized least-squares inversion to estimate the uppermost mantle parameters. The results reveal features that correlate well with the geology and the active tectonics of the region. Overall, the Pn velocities show very fast (>8.4 km s^{-1}) and very slow (<7.6 km s^{-1}) anomalies indicating a heterogeneous lithospheric structure. Relatively uniform Pn velocities (7.9–8.1 km s^{-1}) are observed in western Turkey. The lowest velocities coincide with the volcanics of the easternmost Anatolia and the Central Anatolian Volcanic Zone. High Pn velocities are observed at Mediterranean Basin (>8.3 km s^{-1}), western Black Sea Basin (>8.3 km s^{-1}), Adriatic Sea (>8.3 km s^{-1}) and Zagros Suture (>8.3 km s^{-1}). Pn anisotropy has maximum amplitude of ± 0.6 km s^{-1} in the study area. The largest and coherent anisotropic anomalies are observed in the western Anatolia, Aegean Sea and Cyprian Arc. Pn anisotropy in western Anatolia, Aegean Sea and Greece correlate well with the present deformation of N–S regional extension. No clear correlation between anisotropy and the shear deformation along the North Anatolian Fault was observed. The majority of the stations in central Anatolia show small station residuals indicating the average crustal thickness of 35 ± 2 km. Western Anatolia and the Aegean Sea have crustal thicknesses between 28 ± 2 and 33 ± 2 km. In Greece, the crustal thicknesses are increasing from 33 ± 3 km from the western coast to a maximum of 48 ± 3 km beneath Dinarides-Hellenides. The large crustal thicknesses are also observed along southern coast of Anatolia (40–48 km).

Key words: Tomography; Composition of the mantle; Seismic anisotropy; Seismic tomography; Crustal structure.

INTRODUCTION

Knowledge of the composition and the thermal state on the Earth's mantle is important to better understand the geodynamic behaviour of the lithosphere. For several decades, seismic velocities have been used to determine the physical properties of mantle and much effort has been put into the understanding of the sensitivity of seismic velocities to the changes of mantle composition. Such changes have been investigated at several laboratory studies (Karato & Jung 1988; Sato *et al*. 1989; Watanabe 1993; Karato 1995; Carlson *et al*. 2005) and by observations of various tectonic environments (Eberhart-Phillips *et al*. 2006; Rossi & Abers 2006; Zheng & Lay 2006; Wagner *et al*. 2008).

Pn tomography has proven to be very useful to investigate the uppermost mantle velocity and anisotropic structure at local and regional scales (Hess 1964; Backus 1965; Hearn & Ni 1994; Hearn 1996, 1999). Large velocity contrast between crust and mantle confines propagation of Pn waves to the uppermost mantle and mapping of the lateral variations in Pn velocities using traveltime observations can identify regions with particular importance in dynamic processes, for example partial melt, detachment of subducting plates and presence or absence of mantle lid. In addition, Pn anisotropy allows investigating the strain field in the uppermost mantle as it is sensitive to the preferred orientation of the most abundant upper-mantle minerals, for example olivine and orthopyroxene (Nicolas & Christensen 1987; Christensen 2004).

The structure of the uppermost mantle in Anatolian–Aegean domain has been of interest to many as the region is one of the most active tectonic zones in the eastern Mediterranean. Hearn & Ni (1994) determined Pn velocity distribution for the Turkish–Iranian Plateau. They obtained low Pn velocities (<7.9 km s^{-1}) beneath most of the Turkish–Iranian Plateau and high Pn velocities (>8.1 km s^{-1}) beneath the Black Sea and southern Caspian Sea. Average Pn velocities (8.0–8.1 km s^{-1}) beneath southwestern Mediterranean were observed. Hearn (1999) computed Pn velocity distribution beneath the European region and part of the Aegean Sea. He obtained

much lower seismic velocities (7.6–8.1 km s^{-1}) beneath tectonically active mantle of southern Europe than the more stable mantle of the sub-African Plate of Adriatic Sea (8.3 km s^{-1}).

A more recent study on Pn tomography was performed by Al-Lazki *et al*. (2004). Pn velocities and anisotropy were obtained at the junction of the Arabian, Eurasian and African plates. They observed large scale (∼500 km) low Pn velocity structures (<8.0 km s^{-1}) underlying the Anatolian Plate. Smaller scale (∼200 km) very low Pn anomalies (<7.8 km s^{-1}) are observed in central Turkey. The most recent study is done by Gans *et al*. (2009) in a relatively smaller area and data set in central Turkey. They observed very low Pn velocities (<7.8 km s^{-1}) on the eastern part of the North Anatolian Fault Zone (NAFZ) and faster velocities (>8.1 km s^{-1}) on the western part of the fault. Other tomographic studies at various resolutions and scales were also computed in the region (Karagianni *et al*. 2005; Pasyanos 2005; DiLuccio & Pasyanos 2007; Cambaz & Karabulut 2010). Studies on the crustal thickness variations are available in regions at smaller scales (Sodoudi *et al*. 2006; Zhu *et al*. 2006; Zor *et al*. 2006).

The recent improvements on the number and quality of seismic stations in Turkey and surrounding regions have provided high quality seismic data and improved coverage for most of Anatolian and Aegean domain. The approach in this work is similar to Hearn (1996, 1999) and Al-Lazki *et al*. (2004) but benefits from the improved coverage of stations and data quality. From 1999 to 2010, a total of 700 earthquakes with magnitudes greater than 4.0 are selected. Pn arrivals are defined as the first arrivals between 180 and 1500 km distance range. More than 50 000 Pn arrivals recorded by 832 stations were used for tomographic imaging. We computed both isotropic and anisotropic Pn velocity distributions and estimated crustal thickness variations. Pn velocities are found to be lowest in eastern Turkey (<7.6 km s^{-1}) and highest in the eastern Mediterranean Sea and Zagros Suture (>8.3 km s^{-1}). An anomalous low velocity zone is observed in central Anatolia. Large Pn anisotropy is observed in the Aegean, central Anatolia and along the southern coast of Anatolia. The direction of the anisotropy in the Aegean Sea is consistent with the results of geodetic measurements and SKS splitting directions, aligned on the N–S direction in the extensional regime of western Anatolia. The station delays are found to be proportional with the crustal thickness and the crustal thickness estimates are mostly consistent with previously known values. Large crustal thicknesses are observed along the Dinarides-Hellenides and along the southern coast of Anatolia.

TECTONICS AND GEOLOGY

Turkey is an E–W trending segment of the Alpine–Himalayan orogenic belt and located on the boundary between Gondwana in the south and Laurasia in the north. Within this belt different continental and oceanic assemblages related to the opening and closure of the Palaeozoic and Mesozoic oceanic basins collectively named as the Tethys Ocean stuck together with younger igneous, volcanic and sedimentary rocks (Şengör *et al*. 1981; Göncüoğlu *et al*. 2000; Okay 2008). Although the geometry and evolution of the Tethys Ocean is still in debate, there is a consensus regarding the presence of Palaeotethys on the south and Neotethys on the north. Two major E–W trending ophiolite belts indicate the closure and destruction of Neotethys (Stampfli 2000). The northern Neotethys is located between the Sakarya Zone in the north and the Anatolian–Tauride Platform in the south. The southern Neotethys which separated Arabian Platform in the south from Anatolide–Tauride Platform in the north is located along the southeast Anatolian Suture (Okay 2008). The present tectonics of the region follows closure and the destruction of the Neotethyan oceans (Fig. 1).

The tectonic evolution of the region can be defined at several key stages. In the Early Miocene–Late Oligocene, the collision of the Arabia with Eurasia occurred along the Bitlis-Pontides belt resulting with the closure of Bitlis Ocean, a part of the southern Tethys (Facenna *et al*. 2006). A large portion of the collisional belt in the Upper Miocene was uplifted to an elevation of 1.5–2.0 km and a widespread volcanism was observed as a result of the delamination of mantle lithosphere and slab break-off (Keskin 2003; Şengör *et al*. 2003).

Following the uplift of the Turkish–Iranian Plateau, the northward motion of Arabia gave rise to the westward escape of the Anatolian Block along two intracontinental transform faults, the NAF and the East Anatolian Fault (EAF). The NAF which forms the northern boundary of the Anatolian–European plates is a right lateral strike-slip fault and runs for about 1500 km from eastern Anatolia to the Aegean Sea where it splits into several branches (Barka & Kadinsky-Cade 1988; Şengör *et al*. 2005). Geodetic data indicates that the present-day motion of Anatolia with respect to Eurasia is almost totally accommodated by the NAF (Reilinger *et al*. 1997; McClusky *et al*. 2000). Along the boundary of the Anatolian Block with the Arabian Plate, the EAF, a major left lateral strike-slip fault activated during the Late Miocene extends from the northern end of the Dead Sea Fault (DSF) to the eastern end of the NAF (Arpat & Şaroğlu 1971).

As the continental collision was active in the east, the extension was taking place in the eastern Mediterranean region. Crustal thickening and subsequent extension and magmatism followed the closure and the destruction of the Neotethyan oceans (Taymaz *et al*. 2007). The rapid extension has thinned the crust from 45–50 km down to 28–32 km (Yılmaz 1997; Saunders *et al*. 1998). The Hellenic and Cyprian trenches have been the major factors on the distribution of deformation in the region. Along the Hellenic-Cyprus trenches the African Plate is subducting NE beneath the Anatolian Plate at varying rates. As a result of subduction roll-back, the overall velocity field of the Anatolian–Aegean Block relative to Eurasia increases towards the Hellenic arc. Large-scale tomographic images suggest that once continuous subducting slab extending from the Hellenic arc to the Bitlis Suture lost its continuity at the depths of least several hundreds of kilometres and was almost totally consumed on the east of Cyprus (Wortel & Spakman 2000; Piromallo & Morelli 2003; Facenna *et al*. 2006; Biryol *et al*. 2011).

Central Anatolia forms a broad transitional tectonic zone between the extensional tectonic regime of the western Anatolia and the strike-slip tectonic regime of the eastern Anatolia (Koçyiğit *et al*. 2000). Most of the geological structures of central Anatolia and the Taurides, including Isparta Angle, have been sourced from the tectonic and magmatic events related to this active convergent plate boundary (Glover & Robertson 1998; Koçyiğit *et al*. 2000). The region is also characterized by ∼13 Ma to recent post-collision related volcanism (Notsu *et al*. 1995). The evolution of these volcanics could be related to a vertical tear in the subducting African Plate (Biryol *et al*. 2010).

DATA AND METHOD

A waveform database for this study was formed from the permanent and temporary stations operated in the region from 1999 to 2010 (Fig. 2). The main source of the data is the National Network of Turkey operated by Kandilli Observatory and

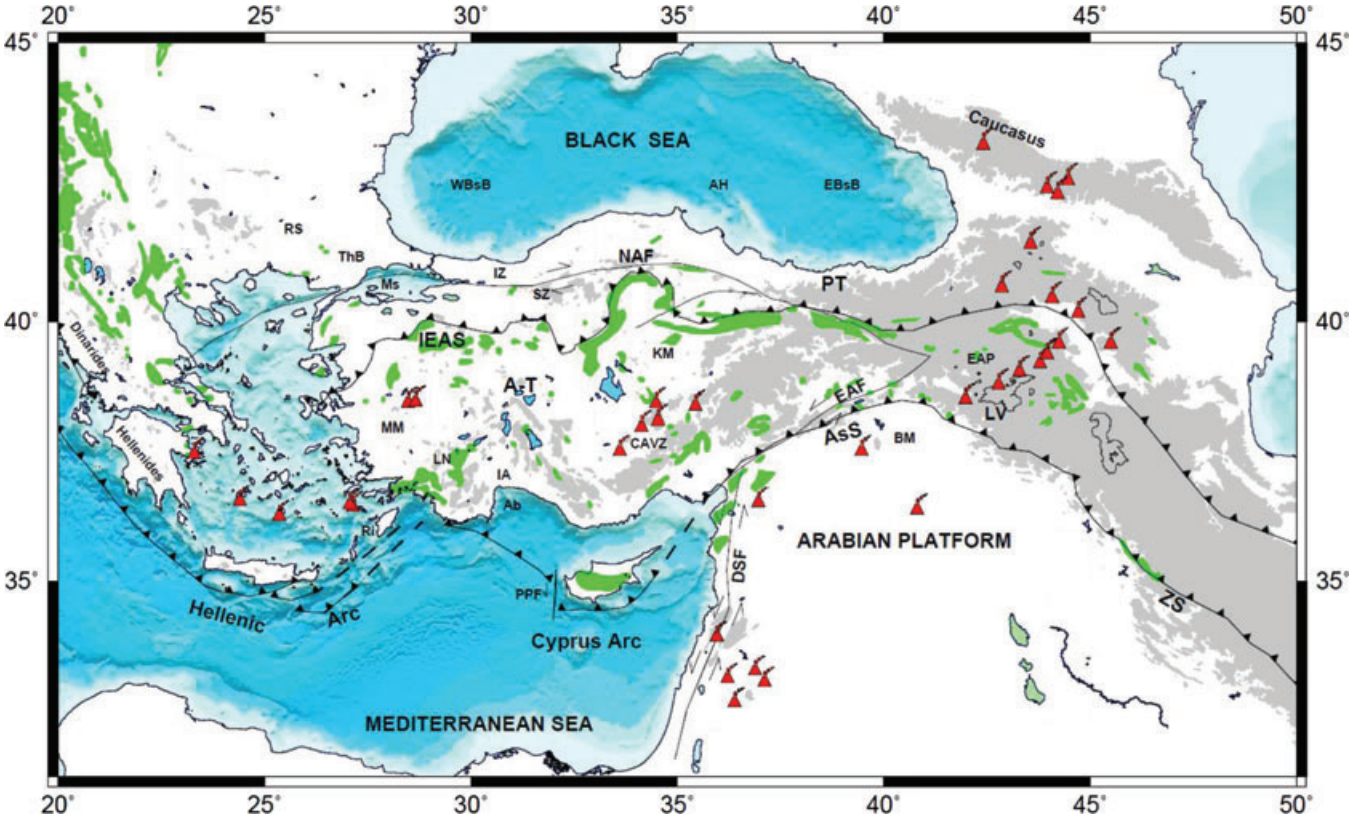

Figure 1. Tectonic map of the study area. Ab, Antalya Basin; A-T, Anatolid-Tauride Block; AsS, Assyrian Suture; BM, Bitlis Massif; CAVZ, Central Anatolia Volcanic Zone; EAF, East Anatolian Fault; EAP, Eastern Anatolia Plateau; EBsB, Eastern Black Sea Basin; DSF, Dead Sea Fault; IA, Isparta Angle; IEAS, Izmir-Eskişehir-Ankara Suture; IZ, Istanbul Zone; MM, Menderes Massif; Ms, Marmara Sea; LN, Lycian Nappes; LV, Lake Van; NAF, North Anatolian Fault; PT, Pontides; PPF, Paphos Transform Fault; RS, Rhodope-Strandja Basin; Ri, Rhodes Island; SZ, Sakarya Zone; ThB, Thrace Basin; WBsB, Western Black Sea Basin; ZS, Zagros Suture. Green and light green units represent the ophiolites and ophiolitic mélanges, respectively. Red volcano signs show Neogene and Quaternary volcanism. Black triangles show the sutures and subduction zones. Black lines indicate the major faults. Grey areas show the elevations greater than 1500 m. Bathymetry and topography of the region derived from ETOPO5 and GTOPO30 (modified from Stampfli, http://www-sst.unil.ch/research/plate_tecto/present_day.htm; Yılmaz *et al*. 1998; Okay & Tüysüz 1999; Robertson 2000; Taymaz *et al*. 2007; Cambaz & Karabulut 2010).

Earthquake Research Institute (KOERI). The network has been continuously upgraded since 2004 and the total number of broadband stations has exceeded 130 in 2010. Supplementary waveform data from IRIS and ORFEUS depositories were obtained for the permanent stations operated in the region. The data from the temporary networks, for example Eastern Turkey Seismic Experiment (Sandvol *et al*. 2003), Western Anatolia Seismic Recording Experiment (Akyol *et al*. 2006) and Seismic Imaging beneath Aegean–Anatolia Domain (SIMBAAD; Paul *et al*. 2008) were also included in the analysis. The observations from several local and aftershock studies were added in the analysis.

The station distribution shown in Fig. 2 is not uniform in the study area. The greater density of the stations is in northwestern Turkey and Aegean and relatively less dense in central and eastern Anatolia. The majority of the earthquakes are located along the active seismic zones such as NAF, EAF and Aegean. Fewer earthquakes were included from Caucasus and Iran.

The initial catalogue for Pn tomography was compiled from the bulletins of KOERI, International Seismological Centre (ISC) and European-Mediterranean Seismological Centre. A total of 700 earthquakes with magnitudes $M_L > 4.0$ were selected and waveform database was constructed for the selected events (Fig. 3). More than 50 000 Pn arrival times recorded at 832 seismic stations were manually picked. The data quality was generally good and only clear Pn arrivals were picked. For ISC bulletin, many Pn are poorly picked and older data may suffer from poor timing. However, these traveltimes constitute less than 5 per cent of the observations. Fig. 4 shows an earthquake gather constructed from the stations located between 27.5°E and 28.5°E for an earthquake approximately located in the middle of the profile.

The locations of the selected earthquakes were improved with manually picked *P* and *S* arrivals at distances smaller than 180 km. The study area was divided into five regions and regional velocity models were constructed using Velest inversion code (Kissling *et al*. 1994). The locations of the earthquakes were computed with these velocity models using the hypocentre location code (Lienert *et al*. 1986). As a result, 596 relocated earthquakes and 695 stations were selected for the analysis. The final selection was based on the location accuracy, focal depths and total number of recording stations. We discarded the events with location errors more than 5 km and hypocentral depths greater than 40 km. We also eliminated stations that recorded less than 10 events and earthquakes with fewer than 10 Pn arrivals. Traveltime residuals greater than 8 s were ignored as the residuals greater than 8 s are significantly larger than the data scatter. As a result, a total of 39 900 Pn travel met the selection criteria and were used for the tomographic analysis.

Fig. 5 shows the reduced traveltimes with a velocity of 8.0 km s^{-1}. The traveltime residuals are varying between ±10 s. Pg and Pn branches of the traveltimes are clearly visible. The critical distance for the data set is observed at ∼180 km. A sharp decrease

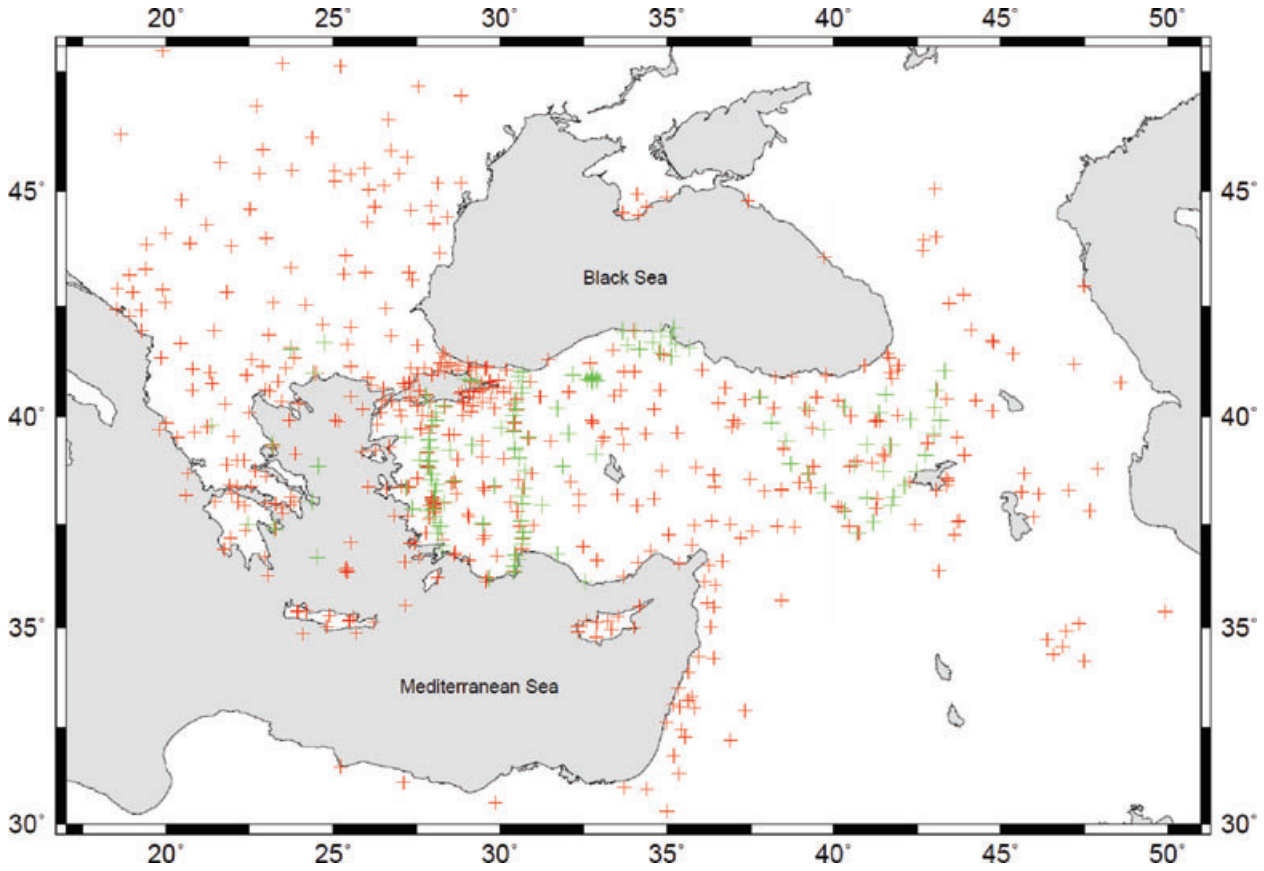

Figure 2. Permanent (+) and temporary (+) seismic stations used for Pn tomography. A total of 695 stations are displayed from both permanent and portable deployments operated between the years of 1999–2010.

in the number of observations is apparent at distances greater than 800 km (Fig. 5). Shorter distances reduce the deviation from the linear path due to the velocity gradient in the mantle lid. Fig. 6 shows ray paths between events and stations. The ray paths provide a good coverage of the study area. The ray density is high in the northwestern Turkey and the Aegean region and relatively less dense in the central and eastern Anatolia. Coverage is poor in the Black Sea, Caucasus and southern Mediterranean.

The Pn traveltime residuals were inverted to determine lateral variations of velocity and anisotropy in the uppermost mantle (Hearn 1999). The method is an extension of the time-term method widely used in the seismic refraction studies (Scheidegger & Willmore 1957; Willmore & Bancroft 1960; Reitter 1970). For the epicentral distances used in this study, the Pn phases are modelled as refracted rays following at crust–mantle velocity contrast. Along the propagation path, Pn paths are separated into three linear segments: the ray path from the source to the mantle, the ray path through the upper mantle and the ray path from the mantle to the receiver. The observed linearity of traveltimes with distance proves the validity of the straight ray paths for refraction path (Fig. 5). The distribution of seismic velocity within the uppermost mantle is parametrized by subdividing the uppermost mantle in a 2-D grid of square cells. Anisotropy perturbation is introduced by a 2θ azimuth variation (Backus 1965; Crampin 1977). The resulting set of equations is solved using a pre-conditioned LSQR conjugate gradient algorithm (Paige & Saunders 1982; Hearn 1996). The convergence is easily attained within 100 iterations. Two damping parameters for slowness and anisotropic coefficients are used to regularize the inverse solution to control the trade-off between errors and resolution. Trade-off between the velocity and the anisotropy is computed from the rms value of the magnitude of the velocity perturbations and the rms of the anisotropy magnitude perturbations for each inversion. The magnitude and the direction of the anisotropy are computed from the coefficients of the terms involving 2θ in the traveltime equation (Hearn 1999).

We determined average uppermost mantle velocity for the data set from a linear fit to the Pn traveltimes in the study area. An average crustal velocity of 6.3 km s^{-1} and crustal thickness of 35 km were obtained from the slope of the Pg traveltimes and intercept time, respectively. These estimates were then used for the initial model of the tomographic inversion. Lateral variations of Pn velocity were imaged as perturbations from the average velocity of 8.0 km s^{-1}. Topography corrections at the station sites were applied assuming a constant velocity of 5.5 km s^{-1}.

Station and event delays were computed relative to the average crustal thickness and velocity of the study area. The station delays are mainly interpreted in terms of Moho depths and the event delays are not interpreted because they are strongly affected by the uncertainties of the depth and the origin time of the earthquakes (Hearn 1996). Station delays depend on crustal, mantle velocities and crustal thickness whereas event delays also take into account errors related to locations. Therefore, crustal thickness and velocity cannot be determined independently from the delay times.

RESOLUTION AND ERROR ANALYSIS

A number of analyses using both real and synthetic data were performed to select optimum cell size, smoothing and weighting

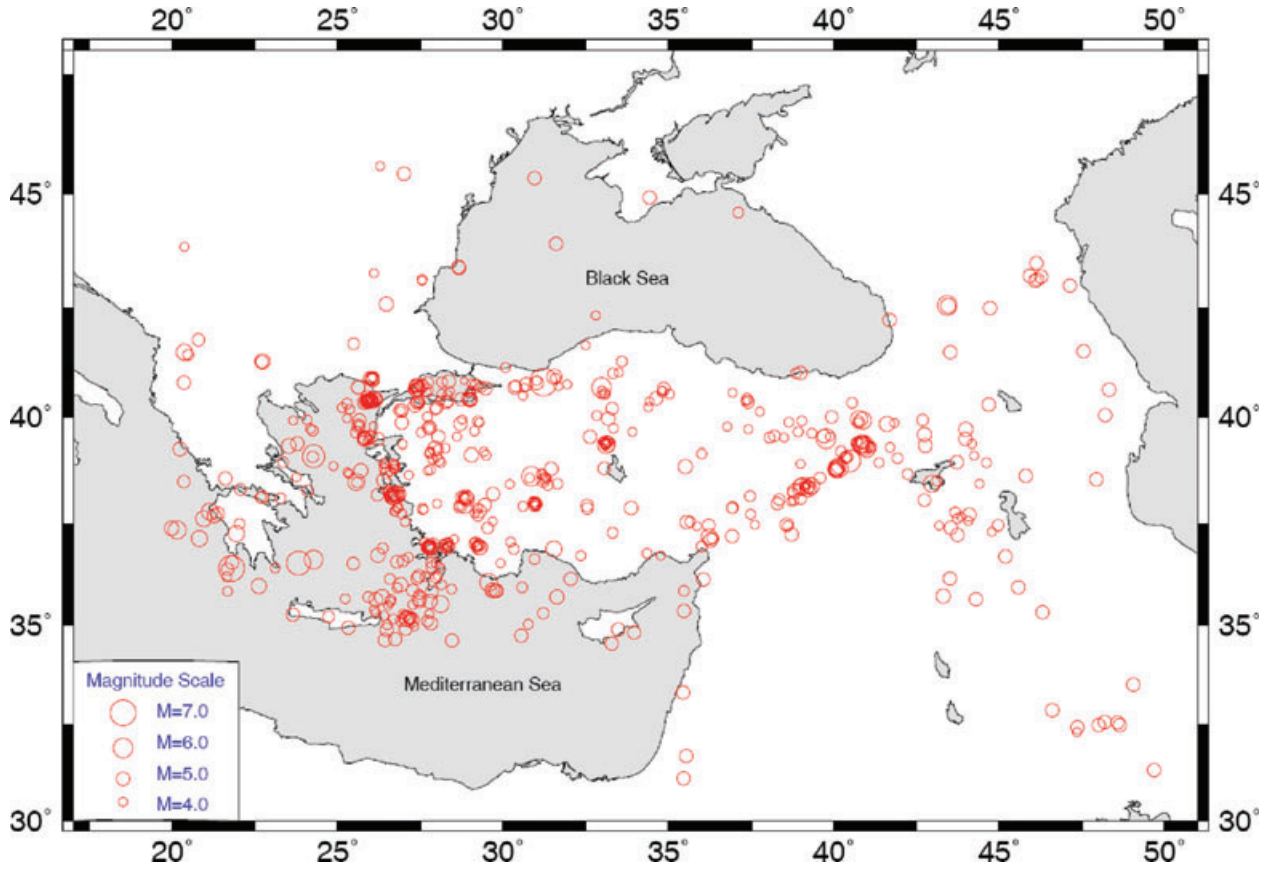

Figure 3. Selected 532 earthquakes (o) for the Pn analysis with magnitudes greater than 4.0 occurred between the years of 1999 and 2010.

parameters. The checkerboard test is the most common way to assess the solution quality, the effect of ray coverage, parametrization of the model space and damping factors. The analysis is performed using the same source–receiver configuration as the observations. Tests are also performed to determine optimum damping parameters. The criterion for selecting optimum parameters is to obtain high level of resolution in which both magnitude and shape of the anomalies are preserved.

The initial checkerboard model for velocity contains alternating values of ± 0.5 km s^{-1} for low and high velocity regions with 1°, 2°, 3° and 4° pattern sizes (Fig. 7). For anisotropy tests, input is a model with 5 per cent variations with fast directions perpendicular in adjacent cells (Fig. 8). The tests are performed for both velocity and anisotropy using damping factors of 200, 400, 600 and 800. Fig. 7 shows the tests on velocity only using a damping factor of 400 to determine the effect of path coverage on various pattern sizes. Fig. 8 shows the tests on anisotropy with a fixed pattern size of 2° and varying damping factors. Both the magnitudes and the shape of the patterns were recovered with pattern sizes greater than 2° in most of the study area (Fig. 7). The result indicate that the patterns smaller than 2° cannot be resolved well in the areas with low ray coverage such as in the Black Sea and the Mediterranean Sea. In the Arabian Plateau the smearing of the patterns also indicates insufficient ray coverage. The resolution depends not only on the ray coverage but also azimuthal coverage. When the azimuthal coverage is poor the anisotropic anomalies cannot be determined accurately. The optimum results from the tests are obtained using damping constants of 400 for the velocity and 400 for the anisotropy.

The determination of measurement errors is important to assess our ability to resolve the observed variations of the Pn velocities. We estimate errors with using bootstrap analysis (Hearn & Ni 1994). Bootstrapping is a way of testing the reliability of the data set and assess whether the distribution has been influenced by stochastic effects. It involves resampling of data with replacement and creates a series of sample data set from the original set. Standard errors of Pn velocity and stations were estimated from the 100 runs.

Fig. 9 shows the result of bootstrap errors for velocity and Fig. 10 for the stations. The velocity errors are low in western Anatolia and the Marmara region (<0.01 km s^{-1}), Aegean Sea (<0.02 km s^{-1}), western Black Sea (<0.04 km s^{-1}) and central Anatolia (<0.05 km s^{-1}). Large values are observed in the eastern Anatolia (>0.08 km s^{-1}), eastern Black Sea (>0.08 km s^{-1}), Arabian Platform (>0.1 km s^{-1}) and Caucasus (>0.12 km s^{-1}). Standard errors of the stations vary between 0 and 1.15 s. In general, large errors (>2 s) at isolated stations are the result of low number of recordings or related to systematic picking errors. These stations were eliminated during the final stage of the inversion.

We computed tomographic images for velocity variations only and velocity-anisotropy together. Fig. 11 shows the inversion with only velocity variations and Fig. 12 show the results for Pn velocity and anisotropy distributions from the combined inversion. The rms errors were 0.98 and 0.93 s for the two inversions, respectively. Fig. 13 shows traveltime residuals before and after the combined inversion with the histograms of the traveltime errors. Significant improvement is observed on the residuals and the variance reduction was 76 per cent. The differences between Figs 11

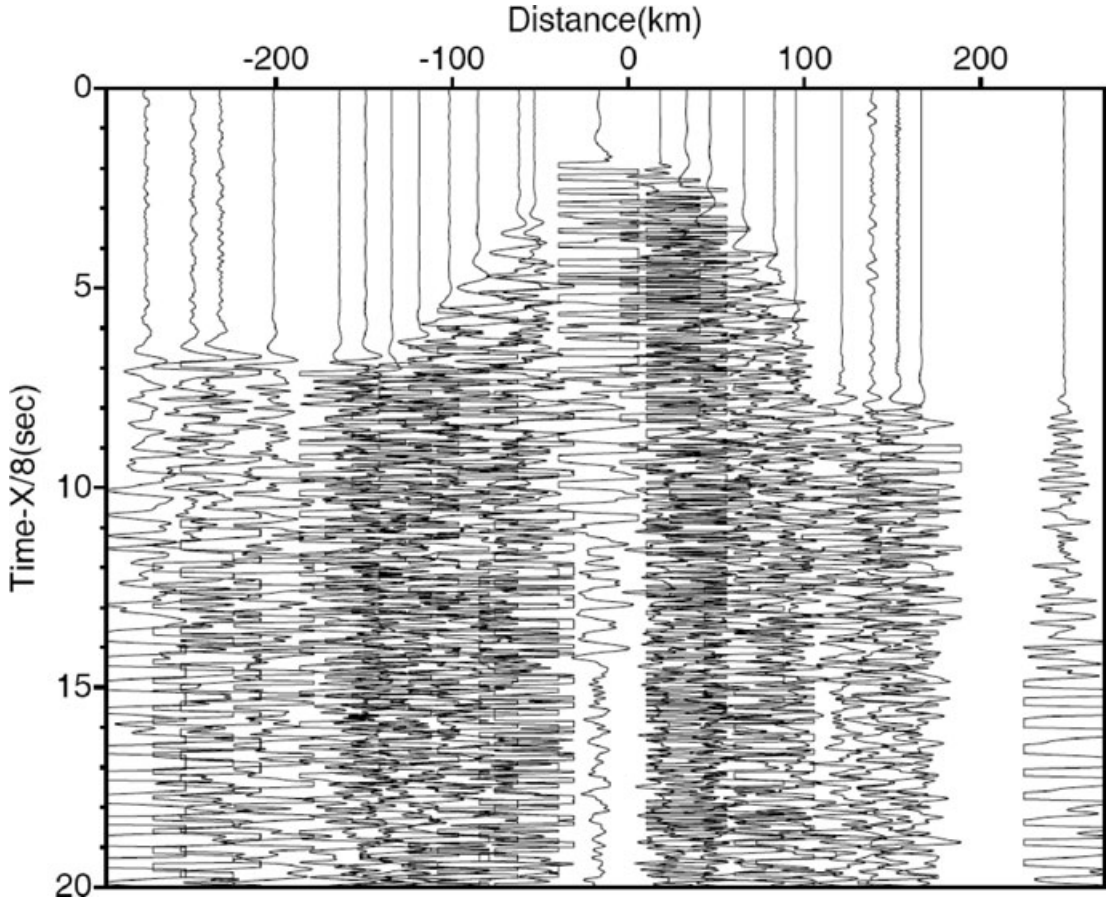

Figure 4. Recordings of an earthquake in western Anatolia. The stations are located between 27.5°E and 28.5°E. The traces are normalized with their maximum amplitudes and plotted with a reduction velocity of 8 km s^{-1}.

and 12 are observed in the low velocity region of eastern Anatolia, along the NAF and the Hellenic arc. The including anisotropy changes the extent and magnitudes of the anomalies but not the locations. The trade-off between velocity and anisotropy may exist in the areas of large velocity contrasts (Figs 14 and 15). Fig. 16 shows stations delays. Station delays for both inversions were nearly identical.

We describe the general features of the Pn inversion and discuss the areas of particular interests in the next subsections.

Pn velocity variations

Large lateral variations in upper-mantle velocities are reported in various tectonic settings (Eberhart-Phillips *et al*. 2006; Rossi & Abers 2006; Zheng & Lay 2006; Wagner *et al*. 2008). These variations mainly result from changes in upper-mantle temperature, composition, presence of water and other volatiles (Karato & Jung 1998; Sato *et al*. 1989; Babuska & Cara 1991; Watanabe 1993; Karato 1995). The laboratory studies on dry peridodite samples, the main constituent of the upper mantle, at high pressure and

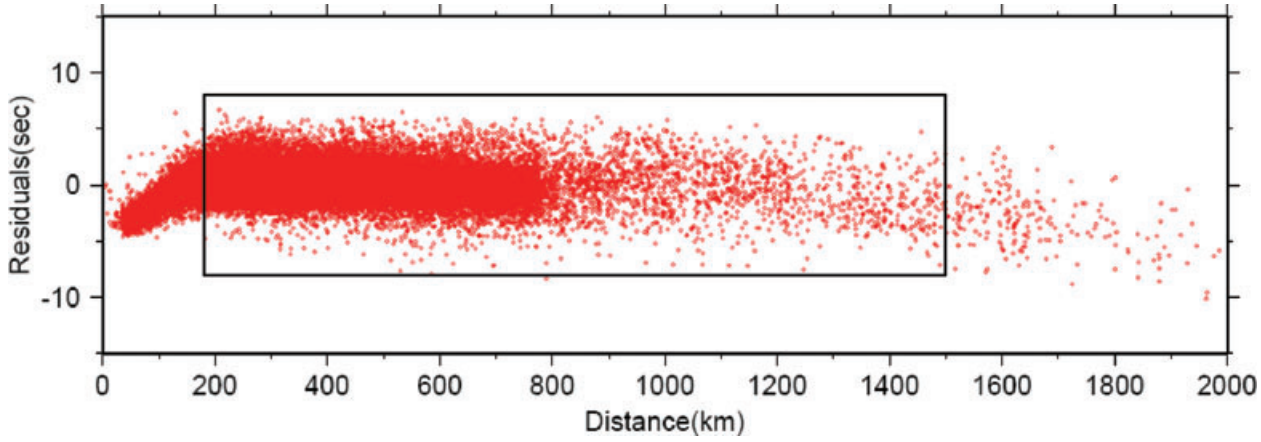

Figure 5. *P* wave traveltime observations at epicentral distances smaller than 2000 km. A reducing velocity of 8.0 km s^{-1} was used. The crossover distance is approximately 180 km. The box shows the range for the observations used in tomography.

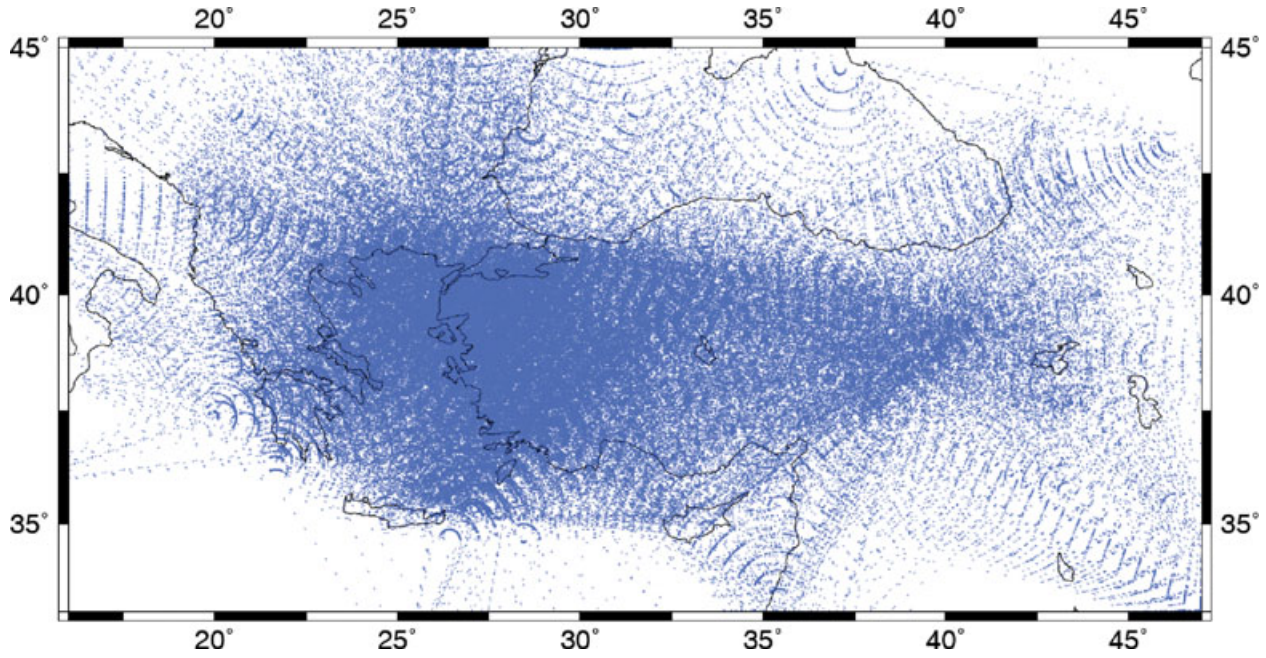

Figure 6. Pn ray paths for tomographic inversion. A total of 532 earthquakes and 695 stations with a grid size of 0.5° × 0.5° were used to compute ray paths. The ray coverage is dense in western Turkey and Aegean while the coverage is low in eastern Turkey, Black Sea and Mediterranean.

temperature indicate that seismic velocities show a rapid decrease with increasing temperature (Sato *et al*. 1989). Small amount of water can contribute to partial melt by reducing the solidus temperature in the mantle (Karato 1995; Karato & Jung 1998).

Overall, the most striking feature of the Pn velocity maps in this study is the observation of very fast and very slow anomalies across the region, which clearly shows the presence of a heterogeneous lithospheric structure (Fig. 12). The Pn velocity is varying from <7.5 to >8.4 km s^{-1} in the study area. High Pn velocities (8.1–8.5 km s^{-1}) are found beneath the oceanic crusts, that is Mediterranean Sea, Hellenic arc, Adriatic Sea as well as Black Sea and Zagros Suture Zone. Velocities are generally higher beneath western Anatolia and Aegean than in eastern Anatolia.

Prominent low velocity anomalies are mainly observed in the east ($>35°$E) of central Anatolia with the lowest Pn velocities are observed beneath eastern Anatolia Plateau (EAP; <7.6 km s^{-1}; Fig. 12). Many of the low Pn velocity anomalies are beneath volcanic regions. Widespread volcanic activity from Upper Miocene

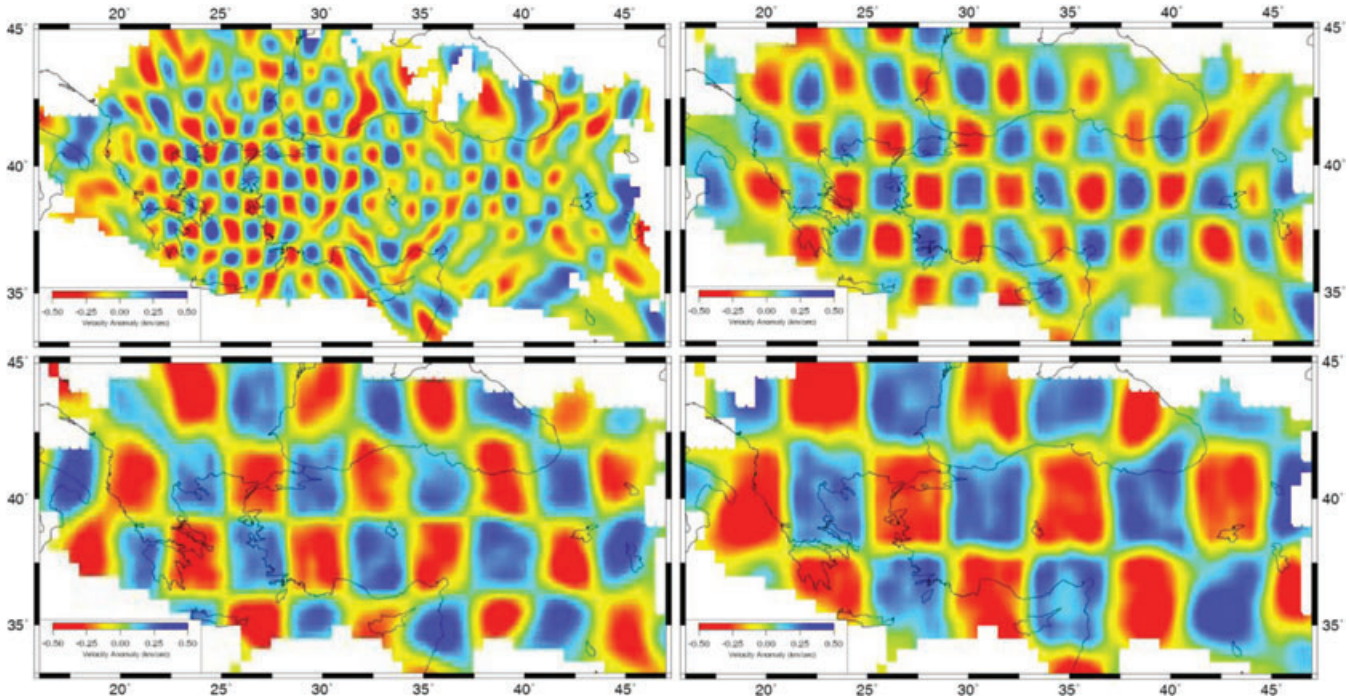

Figure 7. Pn velocity checkerboard tests. Synthetic data are generated with ±0.50 km s^{-1} isotropic velocity perturbations. Recovered isotropic model: starting from upper left to lower right, input pattern sizes are 1°, 2°, 3° and 4°. The damping parameter is assumed as 400.

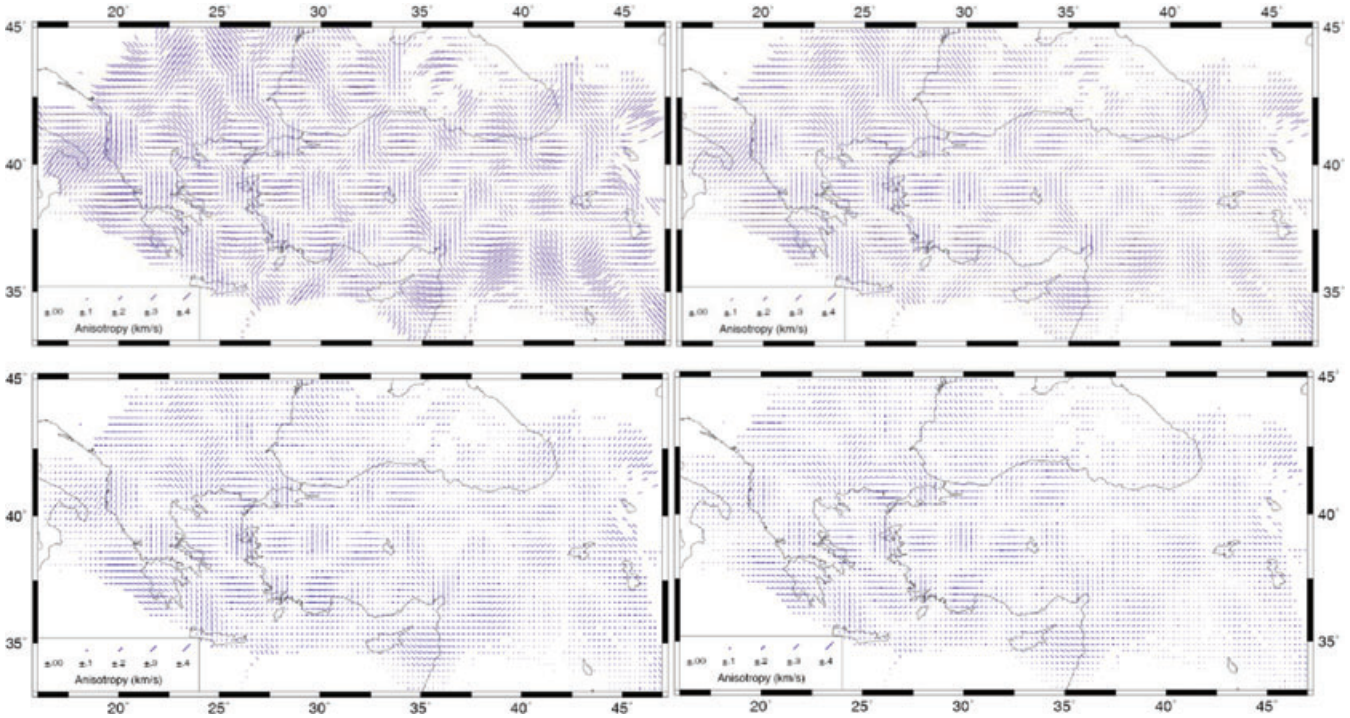

Figure 8. Pn anisotropy checkerboard test. Synthetic data are generated with 5 per cent anisotropy. Anomalies change between ± 0.50 km s^{-1} with a pattern size of 2°. Starting from upper left to lower right, damping parameters are 200, 400, 600 and 800.

to Quaternary is associated with the complete elimination of the Neotethyan ocean floor as a result of collision of Arabia and Eurasia during Early Miocene (Yılmaz *et al*. 1998). The volcanism in the region shows various compositional characters, calc-alkaline in the north and alkaline in the south. Keskin (2003) argued that the subduction component of the volcanics decreases from north to south. This indicates that the volcanism started earlier in the north (∼11 Ma) and migrated to the south (∼2.0 Ma) as a result of the slab detachment beneath the region (Keskin 2003; Şengör *et al*. 2003). The mantle lithosphere was replaced with the low velocity material of asthenosphere beneath the plateau after the detachment of the northward subducting Arabian lithosphere (Keskin 2003; Şengör *et al*. 2003). They suggested that the lithospheric mantle is either thinned or totally removed in the region with the complete destruction of subducting slab. Low velocities in Pn tomography correlate with the volcanic activity in EAP. However, the anomalies do not appear to cover uniformly the entire region but show in two distinct patches with varying magnitudes and sizes. Similar anomalies both

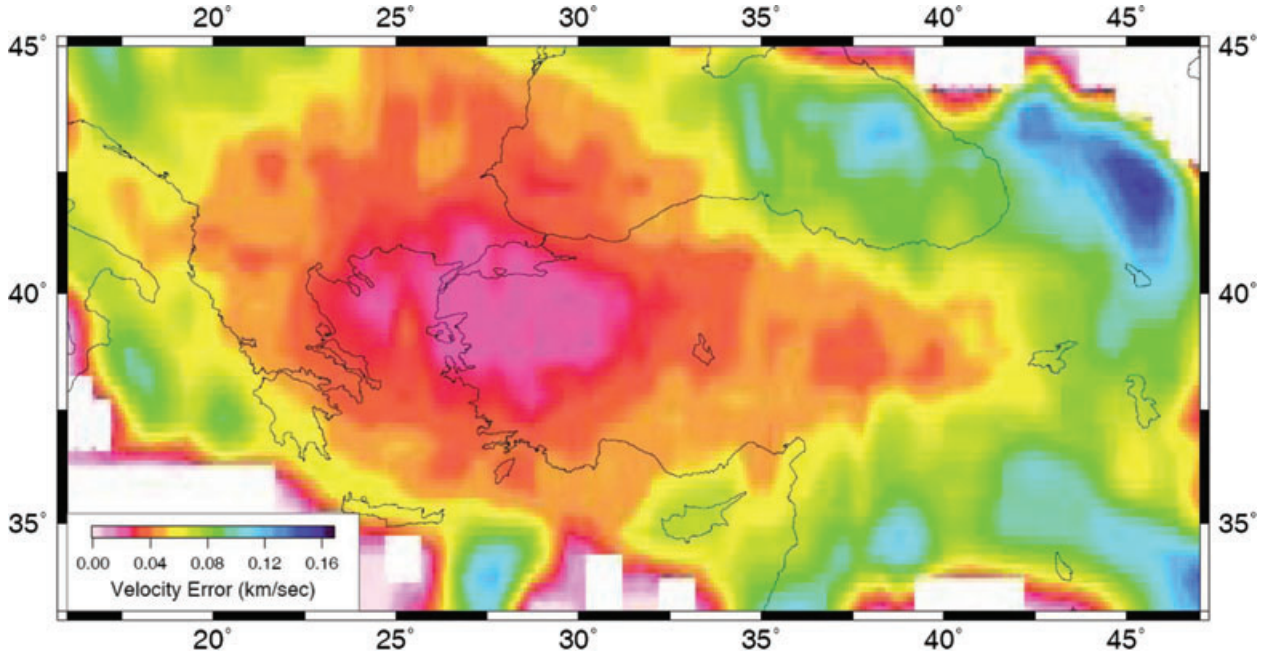

Figure 9. Standard deviations of Pn velocity distribution computed from bootstrap analysis. The deviations are estimated from 100 runs with replacement.

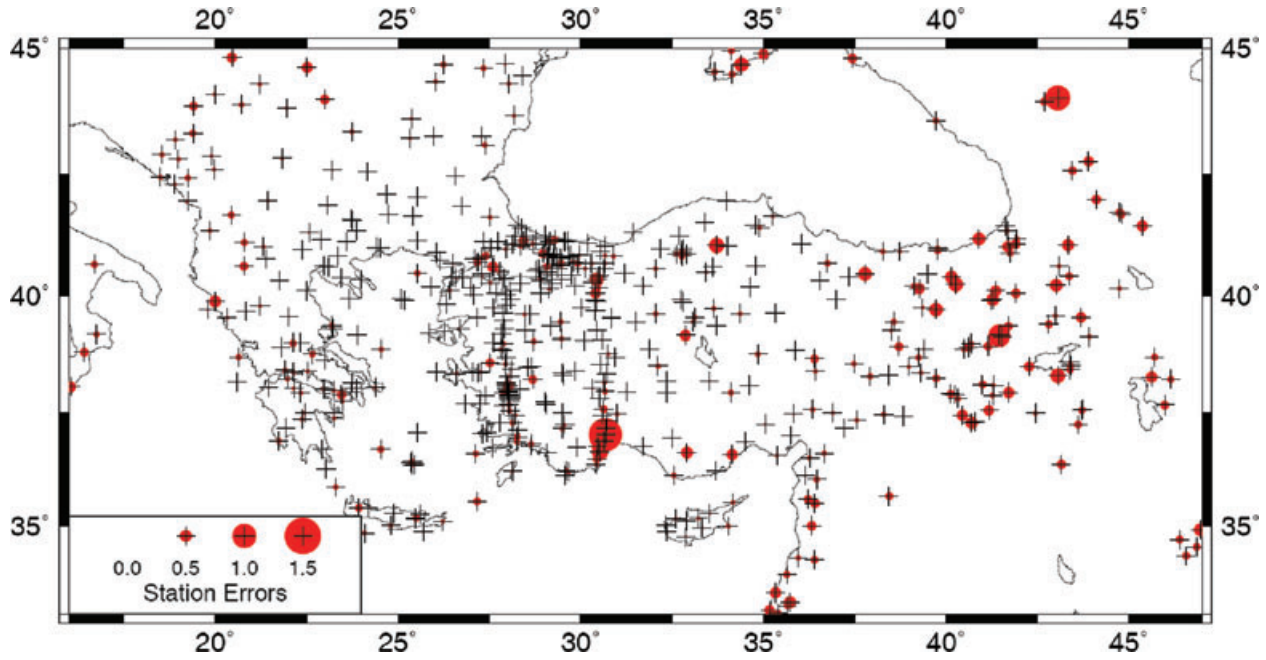

Figure 10. Standard deviations of station delays computed from bootstrap analysis. The deviations are estimated from 100 runs with replacement.

in magnitude and size are also observed by Al-lazki *et al*. (2004). However, in contrary to the previous studies two distinct low velocity zones are separated by relatively higher velocities (7.9–8.0 km s^{-1}). This can be either related to systematic picking errors associated with the attenuation of Pn phases or mantle lid is not completely absent in the region. Another explanation could be the presence of velocity gradient in the mantle.

A prominent low velocity anomaly also appears in Central Anatolia Volcanic Zone (CAVZ; Fig. 12). The low velocities (<7.7 km s^{-1}) coincide with the Neogene–Quaternary volcanism of the area. The tomographic images of Biryol *et al*. (2010) also show slow velocity perturbations as deep as 200 km beneath the CAVZ. However, the low velocities have limited spatial extent in contrast to low velocities of Pn tomography. Pn velocity anomaly covers a larger area and extends towards the low velocities of eastern Anatolia.

The volcanism in the CAVZ is mainly characterized by calc-alkaline and also mild alkaline compositions (Kuşçu & Geneli 2008). The calc-alkaline volcanism is typically observed on convergent plate margins but is not limited only to this tectonic setting (Kuşçu & Geneli 2008). The presence of both calc-alkaline and alkaline magmatism is explained either by opening of an asthenospheric window within the subducting oceanic plate or through channels

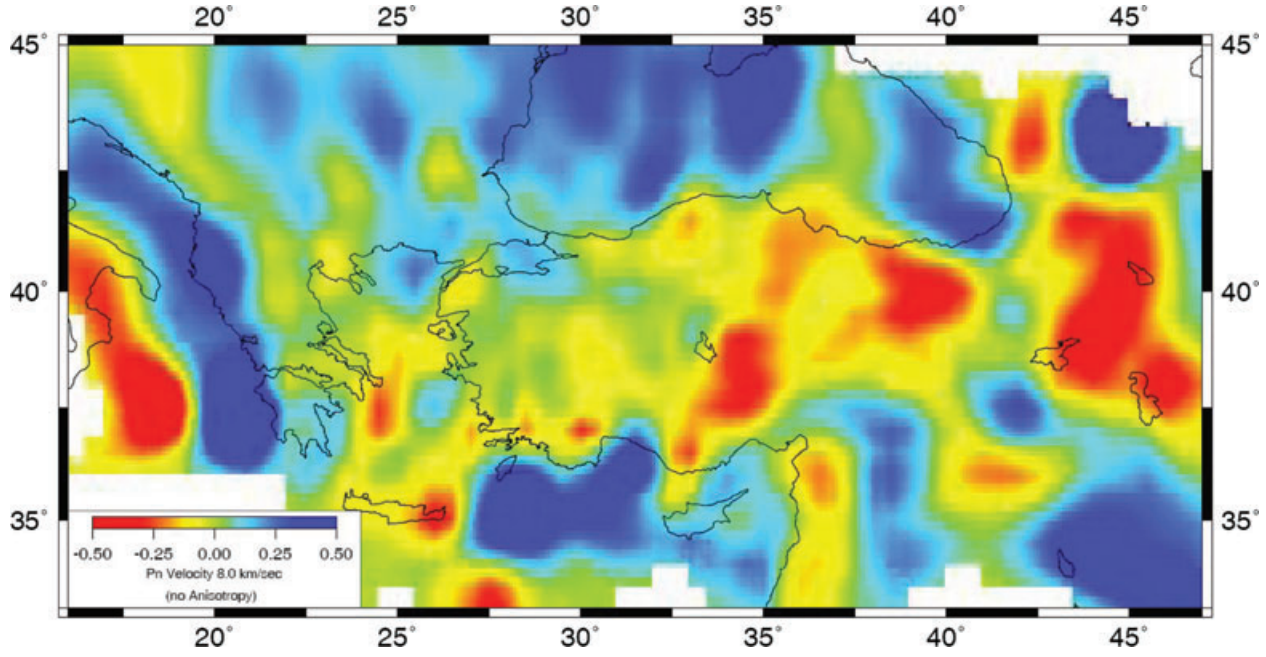

Figure 11. Pn velocity distribution with isotropic model only. Variations from a mean Pn velocity are represented by colours. Only cells with more than 10 arrivals are plotted.

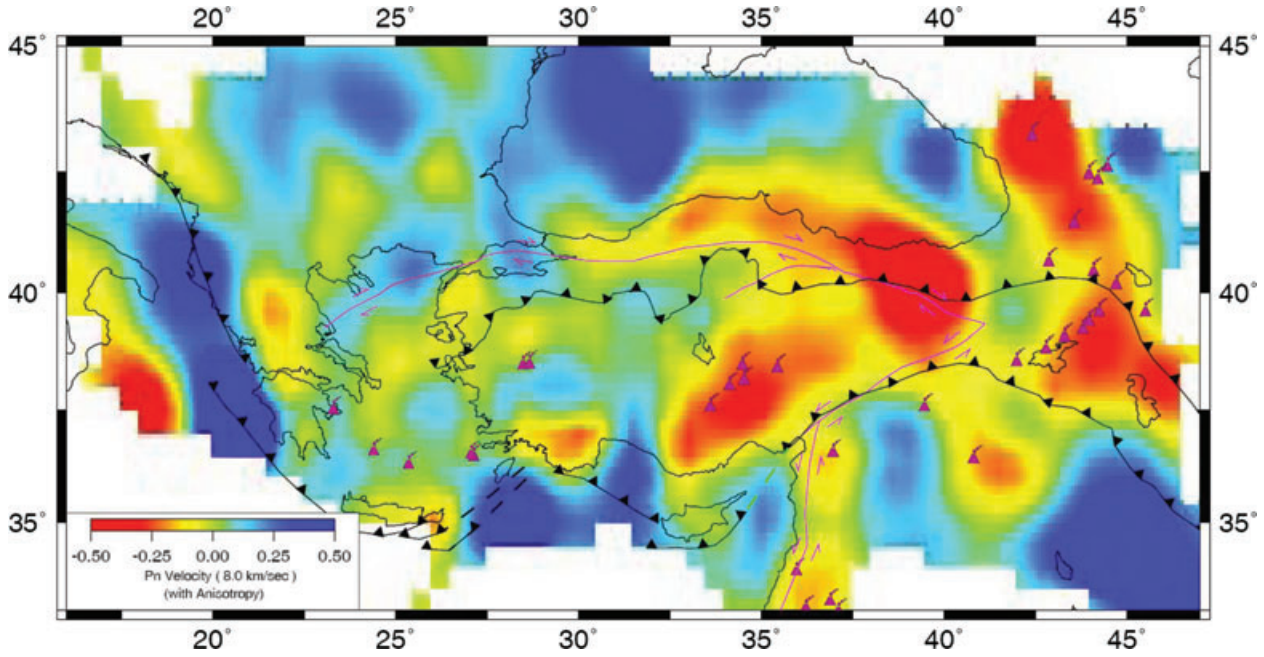

Figure 12. Pn velocity distribution with anisotropy. The fast directions of Pn anisotropy are represented by lines. Only cells with more than 10 arrivals are plotted.

along major lithospheric faults (Pasquare *et al*. 1988; Kuşçu & Geneli 2008). Based on the analysis of the volcanic rocks in the Hasandağı of CAVZ, Deniel *et al*. (1998) also pointed the decreasing influence of the subducted or crustal component through time and the increasing contribution of melt enriched lithosphere. The calc-alkaline character of volcanism in the absence of more recent subduction would indicate the influence of the early subduction of the African Plate under the Eurasian Plate from Eocene to Miocene (Deniel *et al*. 1998). They suggested that the evolution towards alkaline compositions through time is related to the development of extensional tectonics in Central Anatolia in the Late Miocene.

Pn velocities are higher on the south of the Bitlis Suture Zone, boundary between high velocity of the Arabian Platform and low velocity zone of eastern Anatolia. Very high Pn velocities are observed beneath the Zagros Suture Zone ($>$8.3 km s^{-1}). The ray coverage in this region is poor. However, both magnitude and size of the anomaly are so large that the patterns with a size of 3° can be determined and the results are consistent with previous studies (Al-Lazki *et al*. 2004; Kaviani *et al*. 2007).

Lower velocities ($<$7.9 km s^{-1}) are also observed in a narrow range elongating in the N–S direction of the DSF system that forms the plate boundary between Africa and Arabia. The lower velocities there coincide with the Neogene–Quaternary volcanic outcrops observed at the surface. The low velocity region is surrounded by higher velocities of Arabian Platform and Mediterranean Basin (Fig. 12).

Beneath the eastern Mediterranean Basin, Pn velocities are generally higher ($>$8.2 km s^{-1}) but do not show the same strength along the Cyprus and Hellenic belt. The velocities are higher on the west of Cyprus than the east with a sharp transition at Paphos Transform Fault (Fig. 12). The high velocity zone on the west of Cyprus extends from the Paphos discontinuity to Isparta Angle in the N–S direction with decreasing intensity. Further west, a more pronounced high velocity zone ($>$8.4 km s^{-1}) on the south of the Rhodes Island is observed. The two high velocity zones seem to be continuous but the tomographic image has poor resolution on the south. On the north of these high velocity zones, lower velocities ($<$7.8 km s^{-1}) are observed between the Rodhos Islands and the Antalya Bay.

Based on the teleseismic tomography, it is proposed that once continuous subducting slab extending from Hellenic arc to Bitlis Suture have now lost its integrity and is discontinuous (Facenna *et al*. 2006; Biryol *et al*. 2010). The teleseismic tomographic images show the termination of the slab on the east of Cyprus. On the west of Cyprus, a minor tear was located at the Paphos Transform Fault and a major tear was located at the Strabo Transform Zone (Facenna *et al*. 2006; Biryol *et al*. 2010). The low velocity zones could be associated with the flow of low velocity asthenospheric material through the slab tears.

From the 35°E to the Aegean Sea, Pn velocities appear to be relatively uniform. The velocities are varying between 7.9 and 8.1 km s^{-1} with slight decrease on the south and increase on the north. The higher velocities (8.1 km s^{-1}) coincide with the Menderes Massif in western Anatolia and Metamorphic Core Complexes in the Aegean. Western Anatolia is characterized by a broad scale lithospheric extension. Extension started as early as Late Oligocene and widespread by the Late Miocene (Angelier 1978; McKenzie 1978; Le Pichon & Angelier 1981; Şengör *et al*. 1984; Taymaz *et al*. 1991). The GPS surveys show that N–S oriented crustal extension increases in amplitude from north to south (Kahle *et al*. 1998; McClusky *et al*. 2000). Significant crustal stretching and thinning is observed both in western Anatolia and the Aegean Sea. An initial crustal thickness of 45 km is reduced to an average of 33 km since Late Miocene. Metamorphic core complexes observed in the Aegean Sea is a result of such large stretching in the crust. It was pointed out that upper-mantle rocks at high temperatures $>$800 °C become entirely ductile and the viscosity contrast between lower crust and mantle drops significantly (Ribe 1992). As a result the Moho topography remains flat and the mantle velocities are more uniform.

Beneath central Greece and Dinaric-Hellenic Mountain chain, the velocities are low ($<$7.8 km s^{-1}) and there is significant

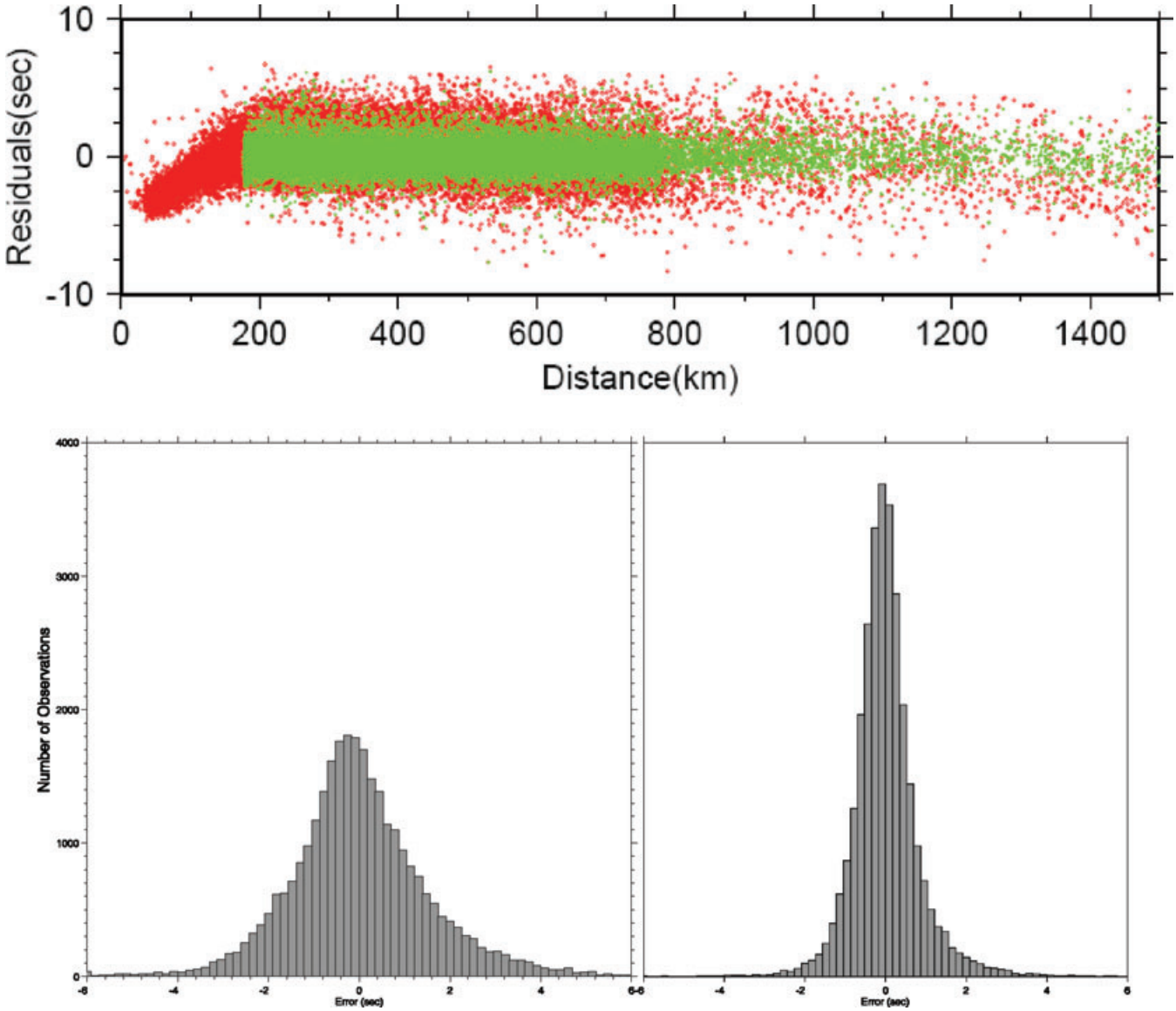

Figure 13. Top: Observed traveltime residuals (red dots) before and after Pn tomography (green dots). A reducing velocity of 8.0 km s^{-1} was used to plot traveltimes. Bottom: Histograms of traveltime errors before (left-hand panel) and after (right-hand panel) inversion.

trade-off between velocity and anisotropy. In the Adriatic Sea, high Pn velocities (>8.2 km s^{-1}) are observed. Similar anomalies are also observed in previous works (Hearn 1999; Al-Lazki *et al*. 2004).

A velocity contrast between Pontides and Anatolia–Taurides is observed along the NAF with lower velocities located on the north (Fig. 12). The contrast is continuous from the eastern part of NAF to the west (>32°E) with decreasing magnitude. This is an indication that the NAF is following the zone of Neotethyan Suture and penetrating into the uppermost mantle (Bozkurt 2001; Şengör *et al*. 2005; Biryol *et al*. 2010). To the west of 32°E, the NAF is crossing a higher velocity zone (>8.1 km s^{-1}) and a velocity contrast across the fault does not appear.

Pn anisotropy

Work on the mantle anisotropy from various tectonic environments present examples of coherent deformation of crust and mantle (Silver 1996; Savage 1999; Polet & Kanamori 2002; Kreemer *et al*. 2004). However, as in the case of the eastern Mediterranean it is not always possible to find such clear correlations. The source of anisotropy in the upper mantle is considered to be the lattice-preferred orientation (LPO) of olivine minerals as a result tectonic deformation (Nicolas & Christensen 1987; Christensen 2004). Deformation tends to align with the fast axis of olivine mineral in the major strain direction (Ribe 1992). Therefore, the coherent deformation of the crust and upper mantle would reflect the latest significant deformation on the mantle. In general, the deformation is parallel to the direction of maximum shearing under a simple shear regime. In subduction zones, the fast axis is parallel to the trench and in backarc regions the fast directions are either parallel or perpendicular to trench. Arc-parallel anisotropy may be due to water in the mantle wedge changing the deformation planes in the olivine (Karato & Jung 1998). The fast axis is parallel to the direction of extension under extensional regime (Silver 1996; Buttles & Olson 1998; Savage 1999; Jolivet *et al*. 2009).

Overall, the anisotropy anomalies observed in this study show a higher level of lateral variations than Pn velocity anomalies

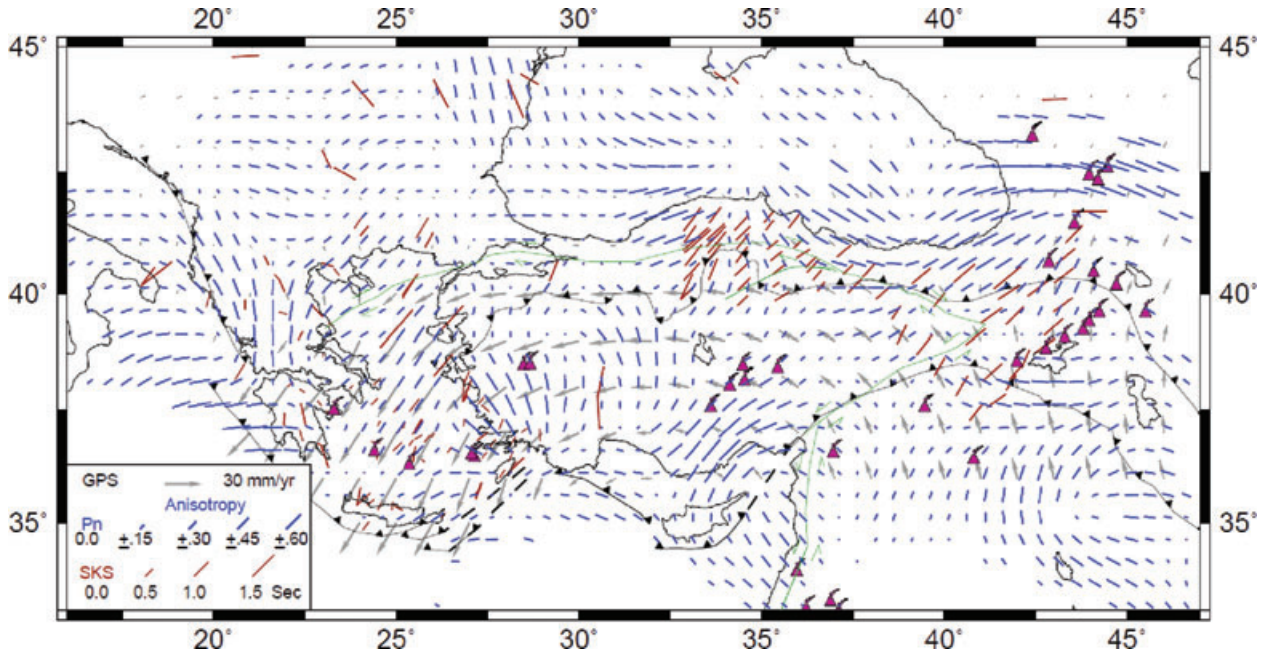

Figure 14. Pn anisotropy in the study area. The blue lines indicate fast direction of Pn velocity. The length of the line is proportional to the strength of anisotropy. The red lines show the SKS fast splitting directions (Hatzfeld *et al*. 2001; Sandvol *et al*. 2003; Biryol *et al*. 2010; Evangelidis *et al*. 2011). The grey vectors indicate interpolated GPS velocities in Eurasia frame (Özeren & Holt 2010). The major faults (green) and plate boundaries (black lines) and volcanoes (triangles) are also shown.

(Fig. 15). A maximum value of 0.6 km s^{-1} which corresponds to about 8 per cent of anisotropy is observed. We obtained large anisotropic anomalies on the southern coast of Anatolia, western Anatolia and central Greece. Large perturbations in anisotropy are observed in the areas of volcanic activity with no clear orientation.

The Pn anisotropy in eastern Anatolia is complex (Fig. 14). Both directions and magnitudes of the fast axis are varying drastically in the region with low Pn velocities (Fig. 15). The anisotropy shows no apparent correlation with GPS velocities and SKS splitting directions (Sandvol *et al*. 2003; Biryol *et al*. 2010). Partial melt might prevent the formation of preferred orientation by promoting a transition from dislocation creep to diffusion creep (Savage 1999). If the thermal evolution of eastern Anatolia as a result of subduction detachment is accepted, the absence of mantle lid could explain the observed anisotropic pattern in the upper mantle.

The anisotropy directions are strongly varying along the southern coast of Anatolia indicating significant influence of the subducting plates. An interesting pattern of the anisotropy takes place in the

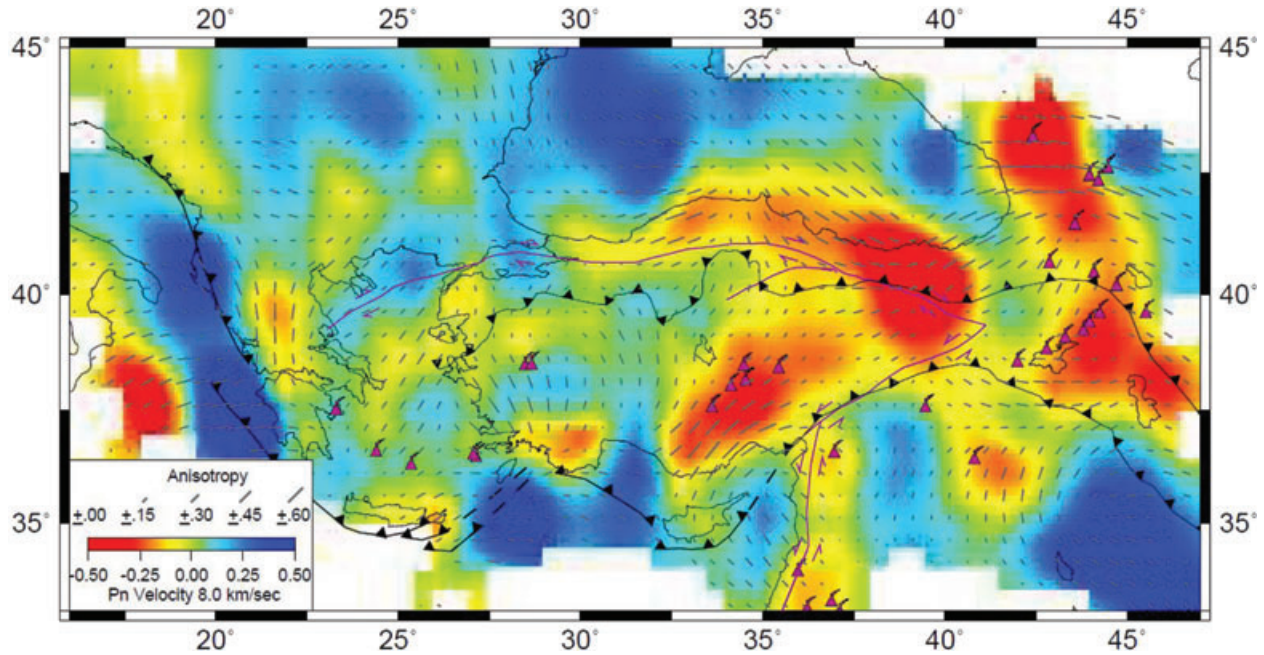

Figure 15. Pn velocity, anisotropy with the major faults and plate boundaries. Pink triangles represent volcanoes.

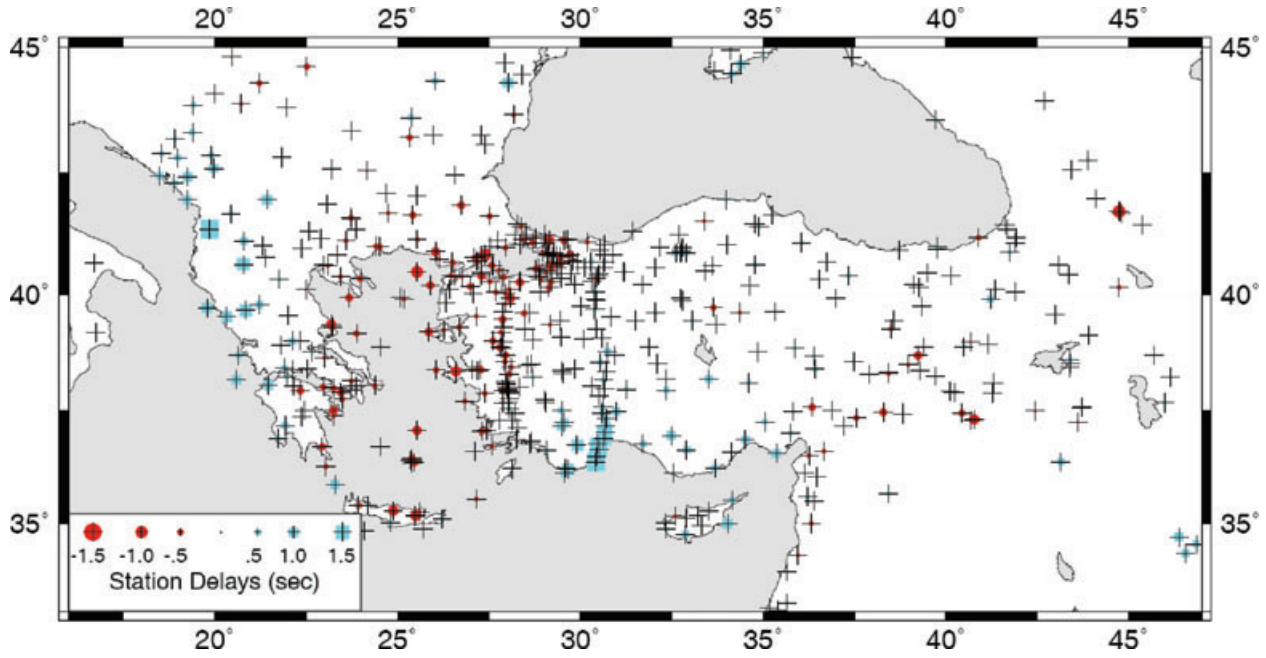

Figure 16. Station delays. Negative delays (triangles) are indicative of a thinner crust (thinner than the average 35 km of the reference model); positive delays (crosses) are indicative of a thicker than average crust.

region of Hellenic-Cyprian arcs and DSF. A strong change on the anisotropy orientations is observed between the DSF and the Paphos Transform Fault. This anomaly is located in a region with the minor slab tear observed in deep tomographic images (Biryol *et al*. 2010). The flow of asthenospheric mantle through the slab tear could be responsible for such anisotropic fabric.

In western Anatolia, the fast axis is almost in the N–S direction and the amplitude is increasing towards the south (Fig. 14). However deviations are apparent from N–S direction in the south which may be related to the subduction geometry and tear in the slab. There is more consistency between the anisotropy directions and the maximum extension directions determined from GPS observations (Aktuğ *et al*. 2009). The magnitude of the anisotropy is quite uniform in the Aegean Sea from north to south and starts diminishing in the area of arc volcanism. Pn anisotropy, SKS splitting directions and GPS vectors are coherent in the Aegean Sea but significantly different beneath the continental Greece (Fig. 14). The fast axis is oriented at NE–SW in the Aegean Sea and N–S in central Greece. Shear wave splitting vectors indicate NE–SW orientations in the Aegean Sea and NW–SE direction in central Greece (Hatzfeld *et al*. 2001). Kreemer *et al*. (2004) indicated that the present-day extension orientations are systematic in northern Aegean and more N–S oriented than SKS splitting orientations and concluded that the current shear-dominated surface deformation pattern is not (yet) reflected by significant anisotropy in the lithosphere. Along the Hellenic-Dinarides belts, the fast axis is oriented in NW–SE direction parallel to the arc. The observed anisotropy is the result of the subduction although it is not active since the Miocene (Hearn 1999).

Central Anatolia shows very small anisotropy between 33°E and 37°E where low Pn velocities are observed (Fig. 15). West of 33°E the fast axis is oriented almost in the N–S direction. Towards north along the Izmir-Eskişehir-Ankara Suture, significant deviations from N–S direction are observed. No clear correlation was observed between the fast axis of Pn anisotropy and the trace of the NAF. The orientation of the fast axis is changing within the central NAFZ from NW in the east to NE in the west.

In the Marmara region, the anisotropy is small and oriented in E–W direction. However, the age of the NAF in the region may not be sufficient to create detectable anisotropic mantle fabric. To reorient LPO in the shear-plane orientation at least 4 Ma are needed and this is consistent with the other observations that the NAF propagated into the Aegean during the Pleistocene (Kreemer *et al*. 2004; Şengör *et al*. 2005). Between Greece and Marmara regions, the fast axis of anisotropy align better with the geometry of the NAF but this may be more related the NE–SW regional extension.

Station delays

Fig. 16 shows the station delays obtained from the tomographic inversion. The station delays provide information only on the relative crustal thickness variations. Early arrivals indicate thicker-slower crust and late arrivals for thinner-faster crust. The station residuals in central Anatolia show very low values (<0.1 s) indicating relatively flat Moho topography. Early arrivals are observed at the stations in Marmara, western Anatolia and Aegean Sea. Large positive delays are sited along the southern coast of Anatolia and Hellenides-Dinarides. In eastern Anatolia positive station delays are observed while very small or negative stations delays are observed on the south of Bitlis Suture Zone.

We computed crustal thickness variations using the station delays. We selected the stations with station errors less than 0.5 s which correspond to ±6 km crustal thickness errors. The selected station delays show non-uniform distribution throughout the region. We used a krigging algorithm to interpolate the station delays for a more uniform distribution. We then converted the station delays to crustal thicknesses. The regional variations of crustal velocities are not known well. We therefore used a constant velocity of 6.3 km s^{-1}. For 1.0 s delay time, the change in the crustal thickness is approximately 11 km and ±10 per cent perturbation of the crustal velocity would

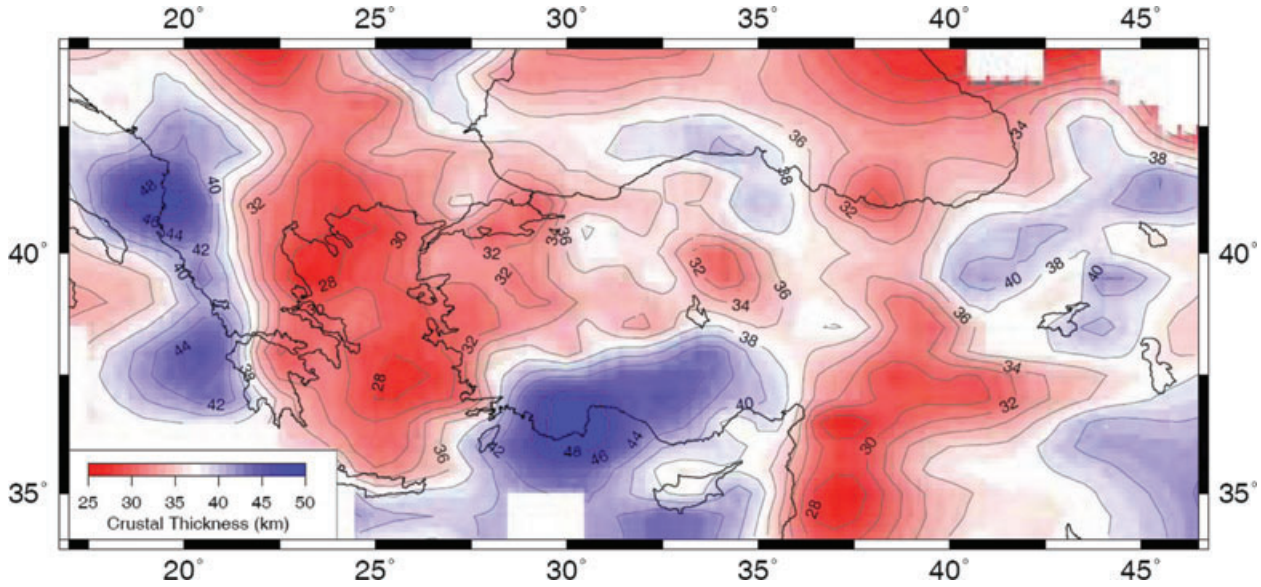

Figure 17. Crustal thickness map obtained from the stations delays. A constant velocity of 6.3 km s^{-1} and 35 km of crustal thickness are used.

result in ±1.5 km change in the thickness assuming an upper-mantle velocity of 8 km s^{-1}. It is important to remember that the crustal thickness determined from the delay time of a station sample an area of ∼70 km in diameter. Additional smoothing imposed by the krigging limits the horizontal resolution.

Fig. 17 shows the crustal thickness variations. Large thicknesses are observed along the southern coast of Turkey (40–48 km) and on the Dinarides–Hellenides arc (40–48 km). In the eastern Anatolia thicknesses are varying from 38 to 40 km. The crust is thinner beneath the Arabian Plateau varying between 32 and 36 km. In the western Anatolia and the Aegean Sea the thicknesses are varying between 28 and 32 km.

In eastern Anatolia, Zor *et al*. (2003) computed crustal thickness between 40 and 48 km. The average crustal thickness is varying from 38 km beneath the Arabian platform to 50 km on the Pontides with a regional average of 45 km (Gök *et al*. 2007). The values obtained in this study are quite lower (40–42 km). The large station errors in the area are the indication of insufficient number of Pn arrivals and the average crustal velocity may not be representative of the region.

In the Marmara region the average crustal thickness is ∼32 km. Laigle *et al*. (2008) obtained the crustal thickness beneath the Sea of Marmara as 26 km and thicker in the east and west of the sea. The receiver function analyses indicate average crustal thickness of ∼30 km on the north of Marmara Sea and increasing to ∼34 km on the south (Zor *et al*. 2006).

The Moho depths in the Aegean are varying between 28 and 32 km. Based on the receiver function analysis, Sodoudi *et al*. (2006) computed crustal thicknesses of 20–22 km on the southern part of the Aegean and found relatively thicker crust (25–28 km) on the northern Aegean Sea. Similar values were obtained by DiLuccio and Pasyanos (2007) indicating an increase of crustal thickness of 20–25 km in the southern and central-western Aegean, whereas reaching 32 km in the northern Aegean.

The crustal thickness obtained from receiver function analysis at Isparta Angle is found ∼42 km, significantly thicker than 35 km in central Anatolia (Zhu *et al*. 2006). The results in this study indicate a significant increase in the crustal thickness from the Isparta Angle (∼39 km) towards the southern coast of Anatolia (∼48 km). Such a large increase can be attributed to the subduction of African lithosphere.

CONCLUSIONS

We presented a new tomographic image of Pn velocities beneath Turkey and surroundings. Both the quality and quantity of the observations provided finer details of the upper-mantle velocity perturbations and anisotropy. The most general feature of the tomographic images is the Anatolian Block characterized by low–moderate Pn velocities surrounded by higher velocities of oceanic crust and often associated with volcanic arcs. The low velocity anomalies observed in the eastern Anatolia is associated with the volcanism following the break off of the subducting oceanic lithosphere. Along the NAF a large velocity contrast but no clear anisotropic orientation related to shear deformation is observed. In western Anatolia and the Aegean Sea, Pn velocities show relatively small perturbations from the average value of 8.0 km s^{-1}. The anisotropy is mostly in the N–S direction and consistent with the regional extension. Both Pn velocity and anisotropy along the coast of southern Anatolia and easternmost Mediterranean shows strong perturbations. These perturbations are related to the present geometry of the subducting slabs and the flow of asthenospheric mantle due to the slab tears. The large crustal thicknesses are estimated along the southern coast of Anatolia and Dinarides-Hellenides. A gradual increase in the crustal thicknesses is observed from the Aegean Sea (28–30 km) to the central Anatolia (35–37 km).

The results presented in this study put more constraints on the active tectonics in the region. The coherence of the Pn anisotropy, SKS splitting directions and GPS velocities show that the Aegean Sea is the only region in the study area that whole lithosphere is deforming coherently. This may indicate that one of the driving forces for the active tectonics beneath the Aegean is mantle flow. In other parts of the region such coherence is not apparent. The mechanisms such as density driven convections (e.g. Faccenna & Becker 2010), smaller scale mantle flow related to slab tears as well as the extrusion of the Anatolian Plate should be considered for a more comprehensive model. More detailed observations on SKS splitting

directions with better density models derived from teleseismic and surface wave tomography will allow us to evaluate the alternatives. The results of the Pn tomography will play important role to validate the hypotheses as it provides the critical information on the deformation between surface observations and mantle flow.

ACKNOWLEDGMENTS

We would like to thank Prof. Thomas M. Hearn for providing Pn tomography code. Critical reviews by Thomas M. Hearn and John F. Cassidy helped to improve the manuscript. Thanks to National Earthquake Information Center of Turkey, IRIS and GEOPHONE for providing the seismic data. Also we would like to thank Dr. Anne Paul for providing the SIMBAAD data (funded by ANR, France, contract 06-BLAN-0317). Some of the figures were generated using the Generic Mapping Tools (GMT) software (Wessel & Smith 1998).

REFERENCES

Aktuğ, B. *et al*., 2009. Deformation of western Turkey from a combination of permanent and campaign GPS data: limits to block-like behavior, *J. geophys. Res.,* **114,** B10404, doi:10.1029/2008JB006000.

Akyol, N., Zhu, L., Mitchell, B.J., Sözbilir, H. & Kekovalı, K., 2006. Crustal structure and local seismicity in Western Anatolia, *Geophys. J. Int.,* **166**(3), 1259–1269.

Al-Lazki, A., Sandvol, E., Seber, D., Barazangi, M., Turkelli, N. & Mohamad, R., 2004. Pn tomographic imaging of mantle lid velocity and anisotropy at the junction of the Arabian, Eurasian and African plates, *Geophys. J. Int.,* **158,** 1024–1040.

Angelier, J., 1978. Tectonic evolution of the Hellenic Arc since the late Miocene, *Tectonophysics,* **49,** 23–36.

Arpat, E. & Şaroğlu, F., 1971. The East Anatolian Fault system: troughs on its development, *Min. Res. Expl. Inst. Turkey Bull.,* **78,** 33–39.

Babuska, V. & Carra, M., 1991. *Seismic Anisotropy in the Earth,* Kluwer Academic Publisher, Dordrecht.

Backus, G.E., 1965. Possible forms of seismic anisotropy of the uppermost mantle under Oceans, *J. geophys. Res.,* **70,** 3429–3439.

Barka, A.A. & Kadinsky-Cade, K., 1988. Strike-slip fault geometry in Turkey and its influence on earthquake activity, *Tectonics,* **7**(3), 663–684.

Biryol, C.B., Zandt, G. Beck, S.L. Özacar, A.A. Adıyaman, H.E. & Gans, C.R., 2010, Shear wave splitting along a nascent plate boundary: the North Anatolian Fault Zone, *Geophys. J. Int.,* **181,** 1201–1213.

Biryol, C.B., Beck, S.L., Zandt, G. & Özacar, A.A., 2011. Segmented African lithosphere beneath the Anatolian region inferred from teleseismic P-wave tomography. *Geophys. J. Int,* **184,** 1037–1057.

Bozkurt, E., 2001. Neotectonics of Turkey—a synthesis, *Geodin. Acta : Eur. J. Geodyn.,* **14**(1–3), 3–30.

Buttles, J. & Olson, P., 1998. A laboratory model of subduction zone anisotropy. *Earth planet. Sci. Lett.,* **164,** 245–262.

Cambaz, M.D. & Karabulut, H., 2010. Love wave group velocity maps of Turkey and surrounding regions, *Geophys. J. Int.,* **181,** 502–520.

Carlson, R.W., Pearson, D.G. & James, D.E., 2005. Physical, chemical, and chronological characteristics of continental mantle, *Rev. Geophys.,* **43,** RG1001, doi:10.1029/ 2004RG000156.

Christensen, N.I., 2004. Serpentinites, peridotites, and seismology, *Int. Geol. Rev.,* **46,** 795–816.

Crampin, S., 1977. A review of the effects of anisotropic layering on the propagation of seismic waves, *Geophys. J. R. astr. Soc.,* **49,** 9–27.

Deniel, C., Aydar, E. & Gourgaud, A., 1998. The Hasan Dağı stratovolcano (Central Anatolia, Turkey): evolution from calc-alkaline to alkaline magmatism in a collision zone, *J. Volc. Geotherm. Res.,* **87,** 275–302.

DiLuccio, F. & Pasyanos, M.E., 2007. Crustal and upper mantle structure in the eastern Mediterranean from the analysis of surface wave dispersion curves, *Geophys. J. Int.,* **169,** 1139–1152.

Eberhart-Phillips, D., Christensen, D., Brocher, T.M., Hansen, R., Ruppert, N.A., Haeussler, P.J. & Abers, G.A., 2006. Imaging the transition from Aleutian subduction to Yakutat collision in central Alaska, with local earthquakes and active source data, *J. geophys. Res.,* **111,** B11303, doi:10.1029/2005JB004240.

Evangelidis, C.P., Liang, W.T., Melis, N.S. & Konstantinou, K.I., 2011. Shear wave anisotropy beneath the Aegean inferred from SKS splitting observations, *J. geophys. Res.,* **116,** B04314, doi:10.1029/2010JB007884.

Faccenna, C. & Becker, T.W., 2010. Shaping mobile belts by small-scale convection. *Nature,* **465**(3), 602–605, doi:10.1038/nature09064.

Faccenna, C., Bellier, O., Martinod, J., Piromallo, C. & Regard, V., 2006. Slab detachment beneath eastern Anatolia: a possible cause for the formation of the North Anatolian fault, *Earth planet. Sci. Lett.,* **242,** 85–97.

Gans, C.R., Beck, S.L., Zandt, G., Biryol, C.B. & Özacar, A.A., 2009. Detecting the limit of slab break-off in Central Turkey: new high-resolution Pn tomography results, *Geophys. J. Int.,* **179,** 1566–1572.

Glover, C. & Robertson, A.H.F., 1998. Neogen intersection of the Aegean and Cyprus Arcs: extensional and strike-slip faulting in the Isparta Angle, SW Turkey, *Tectonophysics,* **298,** 103–132.

Gök, R., Pasyanos, M. & Zor, E., 2007. Lithospheric structure of the continent–continent collision zone: eastern Turkey, *Geophys. J. Int.,* **169,** 1079–1088.

Göncüoğlu, M.C., Turhan, N., Şentürk, K., Özcan, A., Uysal, Ş. & Yalınız, M.K., 2000. A geotraverse across northwestern Turkey: tectonic units of the central Sakarya region and their tectonic evolution, *Geol. Soc. Lond. Spec. Pub.,* **173,** 139–161, doi:10.1144/GSL.SP.2000.173.01.06.

Hatzfeld, D. *et al*., 2001. Shear wave anisotropy in the upper-mantle beneath the Aegean related to internal deformation, *J. geophys, Res.,* **106,** 30 737–30 753.

Hearn, T.M., 1996. Anisotropic Pn tomography in the western United States, *J. geophys. Res,* **101,** 8403–8414.

Hearn, T.M., 1999. Uppermost mantle velocities and anisotropy beneath Europe. *J. geophys. Res.,* **104**(B7), 15 123–15 139.

Hearn, T.M. & Ni, J., 1994. Pn velocities beneath continental collision zones: the Turkish-Iranian Plateau, *Geophys. J. Int.,* **117,** 273–283.

Hess, H.H., 1964. Seismic anisotropy of the uppermost mantle under oceans, *Nature,* **203,** 629–631.

Jolivet, L., Faccenna, C. & Piromallo, C., 2009. From mantle to crust: stretching the Mediterranean, *Earth planet. Sci. Lett.,* **285,** 198–209, doi:10.1016/j.epsl. 2009.06.017.

Kahle, H.-G. *et al*., 1998. The strain field in the eastern Mediterranean region, estimated by repeated GPS measurements, *Tectonophysics,* **294,** 237–252.

Karagianni, E.E., Papazachos, C.B., Panagiotopoulos, D.G., Suhadolc, P., Vuan, A. & Panza, G.F., 2005. Shear velocity structure in the Aegean area obtained by inversion of Rayleigh waves, *Geophys. J. Int.,* **160,** 127–143.

Karato, S.I., 1995. Effects of water on seismic wave velocities in the upper mantle, *Proc. Jpn. Acad.,* **71,** 61–66.

Karato, S.I. & Jung, H., 1998. Water, partial melting and the origin of the seismic low velocity and high attenuation zone in the upper mantle, *Earth planet. Sci. Lett.,* **157,** 193–207.

Kaviani, A., Paul, A., Hatzfeld, D., Vergne, J. & Mokhtari, M., 2007. A strong seismic velocity contrast in the shallow mantle across the Zagros collision zone (Iran), *Geophys. J. Int.,* **171,** 399–410.

Keskin, M., 2003. Magma generation by slab steepening and break off beneath a subduction–accretion complex: an alternative model for collision-related volcanism in eastern Anatolia, Turkey, *Geophys. Res. Lett.,* **30,** 8046.

Kissling, E., Ellsworth, W.L., Eberhart-Phillips, D. & Kradolfer, U., 1994. Initial reference models in local earthquake tomography, *J. geophys. Res.,* **99**(B10), 19 635–19 646, doi:10.1029/93JB03138.

Kreemer, C., Chamot-Rooke, N. & Le Pichon, X., 2004. Constraints on the evolution and vertical coherency of deformation in the Northern Aegean from a comparison of geodetic, geologic and seismologic data, *Earth planet. Sci. Lett.,* **225,** 329–346.

Koçyiğit, A., Ünay, E. & Saraç, G., 2000. Episodic graben formation and extensional neotectonic regime in west Central Anatolia and the Isparta

Angle: a case study in the Akşehir-Afyon Graben, Turkey, *Geol. Soc. Lond., Spec. Publ.,* **173,** 405–421.

Kuşçu, G.G. & Geneli, F., 2008. Review of post-collisional volcanism in the Central Anatolian Volcanic Province (Turkey), with special reference to the Tepeköy Volcanic Complex, *Int. J. Earth Sci.,* **99,** 593–621.

Laigle, M., Becel, A., de Voogd, B. Him, A., Taymaz T. & Özalaybey, S., 2008. A first deep seismic survey in the sea of Marmara: deep basins and whole crust architecture and evolution, *Earth planet. Sci. Lett.,* **270,** 168–179.

Le Pichon, X. & Angelier, J., 1981. The Aegean Sea, *Phil. Trans. R. Soc. Lond.,* **A300,** 357–372.

Lienert B.R., Berg E. & Frazer L.N., 1986. Hypocenter: an earthquake location method using centered, scaled, and adaptively damped least squares, *Bull. seism. Soc. Am.* **76,** 771–783.

McClusky, S. *et al*., 2000, Global Positioning System constraints on plate kinematics and dynamics in the eastern Mediterranean and Caucasus, *J. geophys. Res.,* **105,** 5695–5719.

McKenzie, D., 1978. Active tectonics of the Alpine-Himalayan belt: the Aegean Sea and surrounding regions, *Geophys. J. R. astr. Soc.,* **55,** 217–254.

Nicolas, A. & Christensen, N.I., 1987. Formation of anisotropy in upper mantle peridotites—a review, in *Composition, Structure and Dynamics of the Lithosphere-Asthenosphere System,* pp. 111–123, eds Fuchs, K. & Froideoaux, C., AGU, Washington, DC.

Notsu, K., Fujitoni, T., Ui, T., Matsuda, J. & Ercan, T., 1995. Geochemical features of collision related volcanic rocks in central and Eastern Anatolia, Turkey, *J. Volc. Geotherm. Res.,* **64,** 171–192.

Okay, A.I., 2008; Geology of Turkey: a synopsis, *Anschnitt,* **21,** 19–42.

Okay, A.I. & Tüysüz, O., 1999. Tethyan sutures of northern Turkey, *Geol. Soc. Lond. Spec. Pub.,* **156,** 475–515, doi:10.1144/GSL.SP.1999.156.01.22.

Özeren, M.S. & Holt, W., 2010, The dynamics of the eastern Mediterranean and eastern Turkey, *Geophys. J. Int.,* **183,** 1165–1184.

Paige, C.C. & Saunders M.A., 1982. LSQR: sparse linear equations and least squares problem, *ACM Trans. Math. Softw.,* **8**(2), 195–209.

Pasquare, G., Poli, S., Venzolli, L. & Zanchi, A., 1988. Continental arc volcanism and tectonic setting in Central Anatolia, *Tectonophysics,* **146,** 217–230.

Pasyanos, M.E., 2005. A variable resolution surface wave dispersion study of Eurasia, North Africa, and surrounding regions, *J. geophys. Res*., **110,** B12301, doi:10.1029/2005JB003749.

Paul, A., Hatzfeld, D., Karabulut, H., Hatzidimitriou, P., Childs, D. M. & Nikolova, S., 2008. The Simbaad experiment in W-Turkey and Greece: A dense seismic network to study the crustal and mantle structures, *EOS, Trans. Am. geophys. Un.,* **89**(3), Abstract T21A-1926.

Piromallo, C. & Morelli, A., 2003. P wave tomography of the mantle under the Alpine-Mediterranean area, *J. geophys. Res.,* **108**(B2), 2065, doi:10.1029/2002JB001757.

Polet, J. & Kanamori, H., 2002, Anisotropy beneath California: SKS splitting measurements using a dense, broadband array, *Geophys. J. Int.,* **149,** 313–327.

Reilinger, R.E., McClusky, S.C., Oral, M.B., King, W. & Toksöz, M.N., 1997. Global Positioning System measurements of present-day crustal movements in the Arabia–Africa-Eurasia plate collision zone, *J. geophys. Res.,* **102,** 9983–9999.

Reitter L., 1970, An investigation into the time term method in refraction seismology, *Bull. seism. Soc. Am.* **60**(1), 1–13.

Ribe, N.B., 1992. On the relation between seismic anisotropy and finite strain, *J. geophys. Res.,* **97**(B6), 8737–8747.

Robertson, A.H.F., 2000. Mesozoic-tertiary tectonic-sedimentary evolution of a south Tethyan oceanic basin and its margin in southern Turkey, *Geol. Soc. Lond. Spec. Pub.,* **173,** 97–138, doi:10.1144/GSL.SP.2000.173.01.05.

Rossi, G. & Abers, G.A., 2006. Unusual mantle Poisson's ratio, subduction, and crustal structure in central Alaska, *J. geophys. Res.,* **111**(B9), B09311, doi:10.1029/2005JB003956.

Sandvol, E., Türkelli, N. & Barazangi, M., 2003. The Eastern Turkey seismic experiment: the study of a young continent-continent collision, *Geophys. Res. Lett.,* **30**(24), 8038, doi:10.1029/2003GL018912.

Sato, H., Sacks, I.S. & Murase, T., 1989. the use of laboratory velocity data for estimating temperature and partial melt fraction in the low-velocity zone: comparison with heat flow and electrical conductivity studies, *J. geophys. Res.,* **94**(B5), 5689–5704, doi:10.1029/JB094iB05p05689.

Saunders, P., Priestly K. & Taymaz T., 1998, Variations in the crustal structure beneath western Turkey, *Geophys. J. Int.,* **134,** 373–389.

Savage, M.K., 1999. Seismic anisotropy and mantle deformation: what have we learned from shear-wave splitting?, *Rev. Geophys*., **37,** 65–106.

Scheidegger A.E. & Willmore, P.L., 1957. The use of a least squares method for the interpretation of data from seismic surveys, *Geophysics,* **22,** 9–22.

Şengör, A.M.C. & Yılmaz, Y., 1981. Tethyan evolution of Turkey: a plate tectonic approach, *Tectonophysics,* **75,** 181–241.

Şengör, A.M.C., Satır, M. & Akkok, R., 1984. Timing of tectonic events in the Menderes Massif, western Turkey: implications for tectonic evolution and evidence for Pan-African basement in Turkey, *Tectonics,* **3,** 693–707.

Şengör, A.M.C., Özeren, S., Genç, T. & Zor, E., 2003. East Anatolian high plateau as a mantle supported, north-south shortened domal structure, *Geophys. Res. Lett.,* **30**(24), 8045, doi:10.1029/2003GL017858.

Şengör, A.M.C., Tüysüz, O., İmren, C., Sakınç, M., Eyidoğan, H., Görür, N., Le Pichon, X. & Claude Rangin, C., 2005, The North Anatolian Fault. A new look, *Ann. Rev. Earth planet. Sci.,* **33,** 1–75.

Silver, P.G., 1996. Seismic anisotropy beneath the continents: probing the depths of geology, *Ann. Rev. Earth planet. Sci.,* **24,** 385–432.

Sodoudi, F. *et al*., 2006. Lithospheric structure of the Aegean obtained from P and S receiver functions, *J. geophys. Res.*, **111,** B12307, doi:10.1029/2005JB003932.

Stampfli G.M., 2000, Tethyan oceans, *Geol. Soc. Lond. Spec. Pub.,* **173,** 1–23, doi:10.1144/GSL.SP.2000.173.01.01.

Taymaz, T., Jackson, J. & Mckenzie, D.P. 1991. Active tectonics of the North and Central Aegean Sea, *Geophys. J. Int.,* **106,** 433–490.

Taymaz, T., Yılmaz, Y. & Dilek, Y., 2007. The geodynamics of the Aegean and Anatolia: introduction, *Geol. Soc. Lond. Spec. Pub.,* **291,** 1–16, doi:10.1144.SP291.1.

Wagner, L.S., Anderson, M.L., Jackson, J., Beck, S.L. & Zandt, G., 2008. Seismic evidence for orthopyroxene enrichment in the continental lithosphere, *Geology,* **36,** 935–938.

Watanabe, T., 1993. Effects of water and melt on seismic velocities and their application to characterization of seismic reflectors, *Geophys. Res. Lett.,* **20**(24), 2933–2936, doi:10.1029/93GL03170.

Wessel, P. & Smith, W.H.F., 1998. New, improved version of generic mapping tools released, *EOS, Trans. Am. geophys. Un.,* **79,** 579.

Willmore P.L. & Bancroft, A.M., 1960. The time term approach to refraction seismology, *Geophys. J. R. astr. Soc.* **3,** 419–432.

Wortel, R. & Spakman, W., 2000. Subduction and slab detachment in the Mediterranean-Carpathian region, *Science,* **290,** 1910–1917.

Yılmaz, Y., 1997. Geology of western Anatolia, in *Active Tectonics of Northwestern Anatolia—The Marmara Poly-Project,* pp. 31–53, eds Schidler, C. & Fister, M.P., E.T.H. Univ. Press, Zurich.

Yılmaz, Y., Güner, Y. & Şaroğlu, F., 1998. Geology of the quaternary volcanic centers of the east anatolia, *J. Volc. Geotherm. Res.,* **85,** 173–210.

Zheng, Y. & Lay, T., 2006, Low *Vp* /*Vs* ratios in the crust and upper mantle beneath the sea of Okhotsk inferred from teleseismic *pmP*, *smP*, and *smS* underside reflections from the Moho, *J. geophys. Res.,* **111,** B01305, doi:10.1029/2005JB003724.

Zhu, L., Mitchell, B.J., Akyol, N., Cemen, I. & Kekovali, K., 2006. Crustal thickness variations in the Aegean region and implications for the extension of continental crust, *J. geophys. Res.,* **111,** B01301, doi:10.1029/2005JB003770.

Zor, E., Sandvol, E., Gürbüz, C., Türkelli, N., Şeber, D. & Barazangi, M., 2003. The crustal structure of the east Anatolian plateau (Turkey) from receiver functions, *Geophys. Res. Lett.,* **30**(24), 8044, doi:10.1029/2003GL018192.

Zor, E., Özalaybey, S. & Gürbüz, C., 2006. The crustal structure of the eastern Marmara region (Turkey) by teleseismic receiver functions, *Geophys. J. Int.,* **167,** 213–222.